UNIVERSIDADE D
COIMBRA

André da Silva Pereira

ANÁLISE DA RECUPERAÇÃO DE CALOR EM PROCESSOS INDUSTRIAIS COM UTILIZAÇÃO DE UM SISTEMA ORC

Dissertação no âmbito do Mestrado Integrado em Engenharia Mecânica, Área de Especialização de Energia e Ambiente, orientada pelo Professor Doutor José Manuel Baranda Moreira da Silva Ribeiro e pelo Professor Doutor Márcio Duarte Albino dos Santos, apresentada ao Departamento de Engenharia Mecânica da Universidade de Coimbra.

Julho de 2022

FACULDADE DE CIÊNCIAS E TECNOLOGIA
UNIVERSIDADE D COIMBRA

Analysis of waste heat recover in industrial processes with an ORC system

Submitted in Partial Fulfilment of the Requirements for the Degree of Master in Mechanical Engineering in the speciality of Energy and Environment.

Análise da recuperação de calor em processos industriais com utilização de um sistema ORC

Author

André da Silva Pereira

Advisors

José Manuel Baranda Moreira da Silva Ribeiro

Márcio Duarte Albino dos Santos

Jury

President	**Professor Doutor Ricardo António Lopes Mendes** **Professor Auxiliar da Universidade de Coimbra**
Vowel	**Engenheira Sara Pinheiro Brandão** **Empresa SCIVEN**
Advisor	**Professor Doutor José Manuel Baranda Moreira da Silva Ribeiro** **Professor Auxiliar da Universidade de Coimbra**

Coimbra, July, 2022

A life without festivity is a long road without an inn.

Democritus, around 460-370 BC

To my parents and grandparents.

ACKNOWLEDGEMENTS

My entire academic path of the last 5 years culminated with the development of this work, which would not have been possible without the collaboration, friendship, effort, and patience of several people.

I would like to start by thanking my two advisors, Professor José Manuel Ribeiro, and Professor Márcio Santos for all their support and availability, but above all for their ability to improve me as an engineer.

I also thank all the others who directly helped me develop this work, especially my colleague and friend Engineer Pedro Ferreira for all the support, advice, explanations, adventures, and stories given throughout this work and these last 5 years.

To my colleagues and friends, Paulo Guedes, Pedro Maia and Miguel Gomes for their friendship, strength, patience and feeling of complicity showed throughout my academic career and that I hope will continue after it ends.

To my friends from Marinha Grande and Leiria, Tiago Duarte, Rui Alexandre, Rafael Sá, Leonardo Sá, João Vaz, João Alfaia, Daniel Silva, Vladyslav Yurkevych, Ricardo Roque, Margarida Saboga, Ricardo Oliveira, and Ana Sofia Brandão for all the stories to tell, for all the moments spent and for the friendship, even despite my too prolonged absences.

To Engineer Anselmo Marques for all the teachings, discussions, and future perspectives and for the friendship that remained.

To my mother Ana Paula Silva and my grandparents Maria Alice and Victor Martins for all the education given, for all the effort made and for all the love given so that this goal could be achieved.

To my father Luís Miguel Pereira and my stepmother Marília Lameiro for all the support, love, jokes, dinners, and stories that certainly helped me to distance myself from the problems of everyday life.

I thank all the others I have not mentioned, but who have also accompanied me and will accompany me from now on, in what will be the rest of my life.

Finally, I thank above all those who ever doubted what my academic path or even my life would be and who made me even stronger.

Abstract

One of the objectives defined in the PNEC 2030 and RNC 2050 is to improve industrial energy efficiency, for which waste heat recovery and recycling has already proven to be a good solution. Thus, it is of particular interest to seek to know the existing heat recovery technologies, as well as to evaluate and characterize the potential that waste heat recovery presents either for recycling in industrial processes or to produce thermal, mechanical, or electrical energy. In this work it will be conducted the characterization of waste heat streams with potential to be used in the EU according to the type of industries and their usual temperatures. To conduct this characterization five different studies will be presented.

The Organic Rankine Cycle is one of the main and most interesting systems to produce electrical energy, which is why it served as the basis for the development of a modulating product that recycles waste heat and uses it to produce electrical energy.

Due to the embryonic phase of development of this product and prior to its commercialization and use in real industrial environments, it makes sense to evaluate it against different streams and temperatures typical of such environments.

The second objective of this work was to develop a test stand capable of simulating several waste heat streams with different temperatures and flow rates likely to be found in various industrial conditions. For its development, the natural gas supply line for the laboratory was first dimensioned, followed by the selection of a natural gas burner and the dimensioning of its combustion and mixing/dilution chamber. Finally, a MATLAB model of a compact counter-flow heat exchanger was developed to test which geometric configurations maximize the absorbed power. For the geometries tested the maximum power that could be absorbed was around 110 kW for a combustion power of 195 kW.

After the development of the heat exchanger model, a parametric analysis was conducted, and an evaluation of the absorbed power evolution with the variation of several geometric characteristics.

Finally, the 3D development of the set formed by burner, combustion and mixing/dilution chamber, centrifugal fan, heat exchanger and respective connections was conducted.

Keywords: Energy efficiency, Waste heat, Organic Rankine cycle, Test stand, Heat exchanger, Energy recovery.

Resumo

Um dos objetivos definidos no PNEC 2030 e no RNC 2050 passa por melhorar a eficiência energética industrial, para o qual a recuperação e reciclagem de calor residual já provou ser uma boa solução. Assim, é de particular interesse procurar conhecer as tecnologias de recuperação de calor existentes, bem como avaliar e caracterizar o potencial que a recuperação de calor residual apresenta seja para a reciclagem em processos industriais seja para a produção de energia térmica, mecânica ou elétrica. Neste trabalho será realizada a caracterização dos fluxos de calor residual com potencial de serem utilizados na EU de acordo com o tipo de indústrias e as suas temperaturas habituais. Para realizar esta caracterização serão apresentados cinco estudos distintos.

O Ciclo Orgânico de Rankine apresenta-se como um dos principais e mais interessantes sistemas de produção de energia elétrica, pelo que serviu de base para o desenvolvimento de um produto modelar que recicla o calor residual e o utiliza para a produção de energia elétrica.

Devido à fase embrionária de desenvolvimento deste produto e antes da sua comercialização e utilização em ambientes industriais reais faz sentido testar o mesmo perante diferentes correntes e temperaturas típicas desse meio.

O segundo objetivo deste trabalho passou pelo desenvolvimento de uma banca de ensaios capaz de simular diversas correntes de calor residual com diferentes temperaturas e caudais passiveis de encontrar em diversas condições industriais. Para o desenvolvimento da mesma começou se por dimensionar a linha de abastecimento de gás natural para o laboratório, seguida da seleção de um queimador a gás natural e dimensionamento de uma câmara de combustão e de mistura/diluição. Por fim procedeu-se ao desenvolvimento de um modelo em MATLAB de um permutador de calor compacto em contracorrente, de forma a testar qual/quais as configurações geométricas que maximizam a potência absorvida. Para as geometrias testadas a potência máxima que foi possível absorver ronda os 110 kW para uma potência de combustão de 195 kW.

Após o desenvolvimento do modelo do permutador de calor procedeu-se a uma análise paramétrica do mesmo, e uma avaliação da evolução da potência absorvida com a variação de diversas características geométricas.

Por fim realizou-se o desenvolvimento 3D do conjunto formado por queimador, câmara de combustão e mistura, ventilador centrífugo, permutador de calor e respetivas ligações.

Palavras-chave: Eficiência energética, Calor residual, Ciclo orgânico de Rankine, Banca de ensaios, Permutador de calor, Recuperação de energia.

Contents

LIST OF FIGURES

LIST OF TABLES

LIST OF SIMBOLS AND ACRONYMS/ ABBREVIATIONS

List of Symbols

$\Delta\tilde{h}_i^{\circ}$ – Difference between the enthalpy of formation for a given temperature and its enthalpy of formation for 298.15 K [kJ/mol]

ΔP_{adm} – Maximum allowable pressure variation [mbar]

$\emptyset$ – Dimensionless factor

ρ – Density [kg/m^3]

λ_{ij} – Percentage of primary energy from a process that is lost by waste heat

σ_{ijk} – Factor that incorporates the weight of each industry

η_C – Carnot efficiency coefficient [%]

η_{ES} – Balance factor – Energy service [%]

η_{EL} – Balance factor – Exhausts/Effluents [%]

$\eta_{f,sur}$ – Overall efficiency of the finned surface [%]

η_{OL} – Balance factor – Other losses [%]

ε – Steel roughness factor

A_{ff} – Free-flow area of the fin spacing [m^2]

$c_{p,g}$ – Gases specific heat [kJ/(kg·K)]

d_c – Natural gas corrected density

$D_{calculation}$ – Pipe diameter, before being normalized [mm]

D_h – Hydraulic diameter [mm]

D_i – Normalized pipe diameter [mm]

d_r – Natural gas relative density

e – Height of the helical tube [mm]

E_{ij} – Primary energy consumption from a given source [TWh/year]

f – Friction factor

g – Gravitational acceleration [m/s^2]

G_g – Maximum mass velocity of the gases [kg/(s·m^2)]

h – Difference in elevation between the beginning and the end of the section [m]

h_f – Internal heat-transfer coefficient [W/(m^2·K)]

h_g – External heat-transfer coefficient [W/(m^2·K)]

$h_{g,conv}$ – External/gas-side convective heat-transfer coefficient [W/(m^2·K)]

$h_{g,rad}$ – External/gas-side radiative heat-transfer coefficient [W/(m^2·K)]

H_P – Absolute enthalpy – products [kJ/kg]

H_R – Absolute enthalpy – reactants [kJ/kg]

H_P° - Enthalpy for the standard reference pressure of 1 atm - products [kJ/kg]

H_R° - Enthalpy for the standard reference pressure of 1 atm - reactants [kJ/kg]

j_h - Colburn factor

$L_{critical}$ – Sum of the lengths of the different sections of the pipe that make up the critical path [m]

$L_{eq.max}$ – $L_{critical}$ with a 20% increase [m]

LHV – Lower Heat Value [MJ/kmol]

n_i – Number of moles [mol]

Nu – Nusselt's number

K_i – Local pressure drop factor

p – Pressure [bar]

P_f – Final pressure [mbar]

P_{fc} – Corrected final pressure [mbar]

P_{ff} – Free-flow perimeter of the fin spacing [m]

P_i – Initial pressure [mbar]

$pitch$ – Pitch of the helical tube [mm]

P_m – Average pressure [mbar]

P_{nom} – Burner nominal power [kW]

P_o – Atmospheric pressure [mbar]

P_r – Prandtl's Number

Q_{Burner} – Burner feed rate [m^3/h]

$\dot{Q}_{f,i}$ – Heat transferred in a control volume [W]

Q_{R-P} – Heat done by the system on the neighbourhood [kW]

$Q_{section}$ – Section feed rate [m^3/h]

RA – Ratio between the internal and external heat-transfer area

$R_{f,ext}$ – External thermal resistance resulting from fouling [(m^2·K)/W]

$R_{f,int}$ – Internal thermal resistance resulting from fouling [(m^2·K)/W]

$R_{t_{g,i}}$ – Thermal resistance of the tube wall [(m^2·K)/W]

St – Stanton number

T_c – Cold source temperature [K]

T_h – Hot source temperature [K]

T_n – Absolute normal temperature – 273.15 [K]

T_{st} – Absolute standard temperature – 288.15 [K]

U – Overall heat-transfer coefficient [W/(m^2·K)]

U_P – Absolute internal energy – products [kJ]

U_R – Absolute internal energy – reactants [kJ]

v – flow speed inside the pipes [m/s]

v_f – Final velocity [m/s]

v_i – Initial velocity [m/s]

V_P – Volume – products [m^3]

V_R – Volume – reactants [m^3]

WHF – Waste heat fraction

$WHRP$ – Waste heat recovery potential [TWh/year]

W_{R-P} – Work done by the system on the neighbourhood [kW]

z_f – Elevation at the final point [m]

z_i – Elevation at the starting point [m]

Acronyms/Abbreviations

AHU– Air Handling Unit

CWHRP – Carnot Waste Heat Recovery Potential

EI – Energy Intensity

EU – European Union

GHG – Green House Gas

HT – High Temperature

LMDT – Logarithmic Mean Temperature Difference

LT – Low Temperature

LULUCF – Land Use, Land-Use Change and Forestry

MCV – Mechanical Vapour Compressor

MT – Medium Temperature

ORC – Organic Rankine Cycle

PNEC – *Plano Nacional de Energia e Clima*

RNC 2050 – *Roteiro nacional para a Neutralidade Carbónica*

UC – Universidade de Coimbra

WHF – Waste Heat Fraction

WHR – Waste Heat Recovery

WHRP – Waste Heat Recovery Potential

WHTC – Waste Heat to Cold

WHTH – Waste Heat to Heat

WHTP – Waste Heat to Power

1. INTRODUCTION

1.1. Framework

The industrial development of the past decades allowed for an increase in countries economic power and consequently improved the quality of life of the populations. On the other hand, there has been a sharp increase in world population, a greater need to extract natural resources from the planet, and an unprecedented consumerism. Unbridled and uncontrolled extraction has triggered a consumption of resources beyond the natural replacement capacity. However, the most current and worrying consequence of human activity is the extremely high levels of greenhouse gas (GHG) emissions, resulting from industrial activities, services, housing, transportation, agricultural and livestock activities.

Using Portugal´s statistical data from the last few years (Figure 1.1), it is possible to observe a rapid growth of emissions in the 1990s, with a maximum registered in the year 2005. In this year, a 44% increase in emissions was reached when compared to 1990 [1]. Since then, there has been a small decrease in GHG emissions that results from a greater effort and awareness of governments for climate problems, combined with the measures taken in the Kyoto Protocol, where it was established that Portugal could only increase its emissions by 27% compared to 1990 in the 2008-2012 period [1].

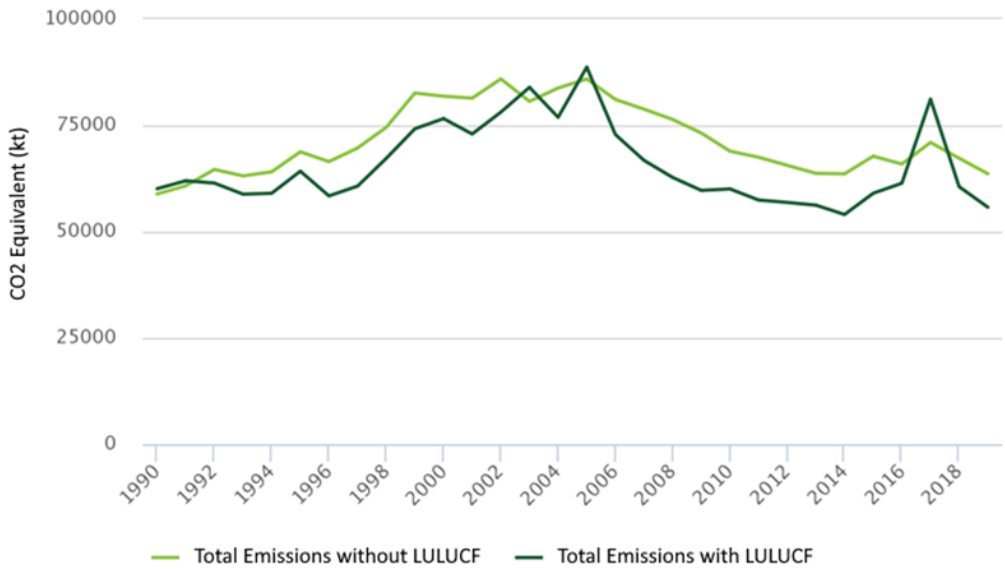

Figure 1.1. Evolution of GHG in Portugal – Adapted from [2].

Based on scientific studies, it was concluded that an increase in global average temperature of 1.5°C is the maximum limit so that there are no changes that are too disruptive to life on Earth. Based on this, the Paris Agreement, reached in 2015, established as a minimum, long-term goal, a containment of the global average temperature increase to 2°C in relation to pre-industrial levels, but with the objective and commitment that this increase is fixed at a maximum of 1.5°C [1].

This agreement exposed an ongoing problem that can only be reversed with the participation and compliance of all states. Portugal is included and presents the goal to achieve carbon neutrality by 2050, developing a set of measures and actions to be implemented within this timeframe [1].

Given the goals set by the country, the "*Roteiro Nacional para a Neutralidade Carbónica (RNC 2050)"* was established, with special emphasis on the decade 2021-2030 for which *"Plano Nacional Energia e Clima 2021-2030 (PNEC 2030)"* was developed [1], [3]. Goals were set for 2030 such as the reduction of CO_2 emissions between 45 and 55%, an increase in energy efficiency by 35%, an increase in renewable energy sources by 47%, 20% increase in the fleet of vehicles powered by renewable energy, and 15% electricity interconnections.

For carbon neutrality to be attainable by 2050 means the progressive abandonment of a linear economic model. This translates into abandoning an economy based on fossil fuels, enabling a transition to an economy based on renewable energy that uses resources efficiently, that is, in a circular economy. This requires joint action in several strategic areas, prioritizing energy efficiency, increasing electrification, strengthening, and modernizing infrastructure, developing interconnections, market stability and investment, reforming market digitalization, and encouraging research and innovation [1].

Portugal has geographical characteristics that allow the development of a fully decarbonized electroproduction sector (water, wind, sun, biomass, geothermal), reliable and secure, able to deal with the variability that the bet on renewable energy brings [1]. This energy transition will apply to all sectors of society: housing, services, industry, and agriculture and livestock. However, this transition will not be sudden and in many cases will be impossible. This is most noticeable when looking at the industry sector, one of the sectors responsible for the largest energy needs in the EU (see Figure 1.2), which due to the nature of some processes involved makes a shift to an electrified base financially and/or

technologically impossible. Thus, in these cases, the focus should be mainly on improving the energy efficiency of industrial processes.

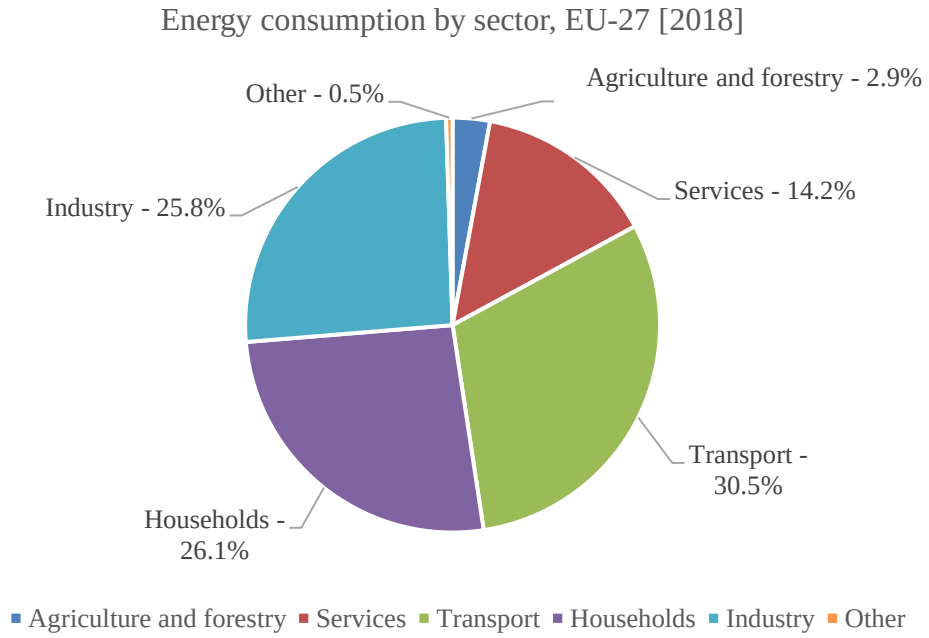

Figure 1.2. Energy consumption by sector, EU-27 in 2018 – Adapted from [4].

Improving energy efficiency in industrial processes is mainly about reducing the specific energy consumption (consumption per unit produced), seeking better energy management, or recovering and using waste heat [5]. A reduction in industrial activity implies a radical change in the business model and is not applicable to all companies. Improving energy management has already proven to be a good solution to increase energy efficiency. The investment in waste heat recovery systems will reduce energy inefficiencies, the consumption per unit produced and consequently companies' energy bills, making them more efficient and competitive in national and international markets. Waste heat can be used to produce useful thermal, mechanical, or electrical energy.

Thus, it is important to continue the study and development of technologies to reduce the energy waste associated with heat and help the country, the EU, and the world to meet the climate goals set, while keeping the industry efficient and competitive.

1.2. State of the Art

This section will provide a brief review of the definitions and concept of waste heat potential and the characteristics of heat sources. In addition, the most used waste heat

recovery technologies will be identified, as well as their typical efficiency and cost in €/kW of recovered heat. A comprehensive introduction to the Organic Rankine Cycle will be made since it is a system of special interest for electrical energy production. Finally, the waste heat streams with the potential to be used in the EU will be characterized, according to the type of industries and their usual temperatures.

1.2.1. Waste Heat Definition

It is impossible to disaffiliate the concept of waste heat from the production of work, since all processes involving work will produce heat, which will be released in the form of radiation, convection (to a refrigerant fluid or to air) and conduction, and through mass transfer by flue gases. Thus, waste heat may appear in all forms of heat: sensible and latent, that are not used by the product, process, or the plant [5], [6]. In fact, the existence of this wasted energy is often associated with the lack of economic added value or non-existent environmental restrictions at the time of the project of a certain installation.

In some cases, waste heat still possesses considerable exergy, so it can be harvested and used to produce work using heat recovery technologies [6]. Waste heat functions as an extra source of energy and can be used to create additional useful heat, generate mechanical or electrical energy [7].

Waste heat recovery is based on the principle that no energy is lost, but rather that all is transformed so there is potential to reuse it, either through a closed cycle where the heat is recycled in the same process or through an extended cycle where the heat is reused for multiple energy needs (Figure 1.3) [7].

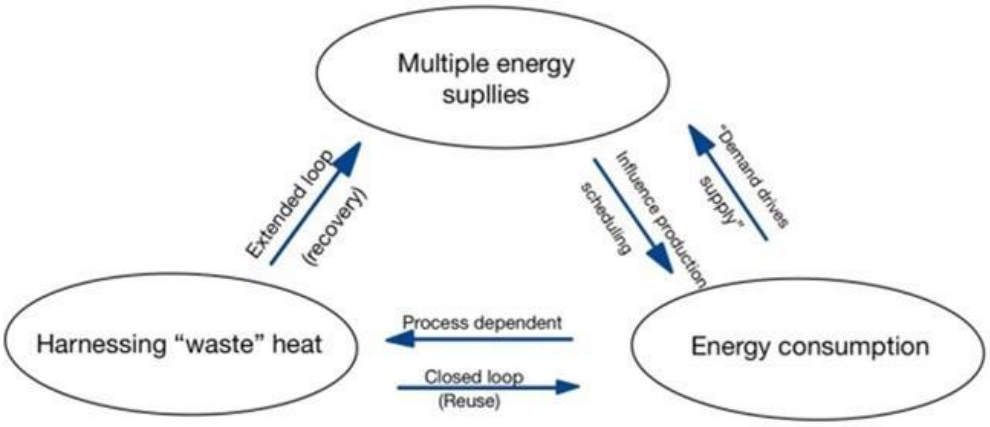

Figure 1.3. Energy and Waste Heat Cycle of a Plant – Adapted from [5].

1.2.2. Theoretical, Technical and Economic Waste Heat Potential

Not all waste heat can be used due to thermodynamic, technical, or economic issues. Therefore, it is necessary to differentiate between the theoretical, technical, and economic potential of waste heat (Figure 1.4).

The theoretical potential only considers physical/thermodynamic constraints, such as if the heat source is at a higher temperature than the ambient temperature, leaving out the heat lost through radiation. Issues such as whether it is possible to extract heat from heat sources or whether it is susceptible to be used in some applications are not considered in the theoretical potential, these issues are addressed in the technical potential [6]. Thus, the technical potential depends on the available heat recovery technologies and technical constraints, such as whether the temperature of the rejected heat is sufficient for heat transfer or whether industries have conditions and particularities for the installation and maintenance of equipment. Finally economic characteristics such as energy prices, rates of return on investment and payback period are considered in the economic potential of waste heat, allowing to assess whether a technology is profitable [8].

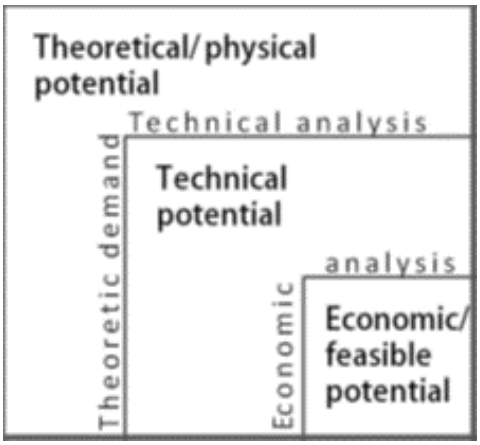

Figure 1.4. Types of Waste Heat Potential [6].

In Panayiotou *et al.* [9] a step forward in distinguishing between theoretical technical potential and applicable technical potential is given. The former is calculated using a technical-theoretical analysis related to the process while the latter is calculated using data specific to each company and each situation. This is translated in Figure 1.5 which corresponds to an evolution of Figure 1.4.

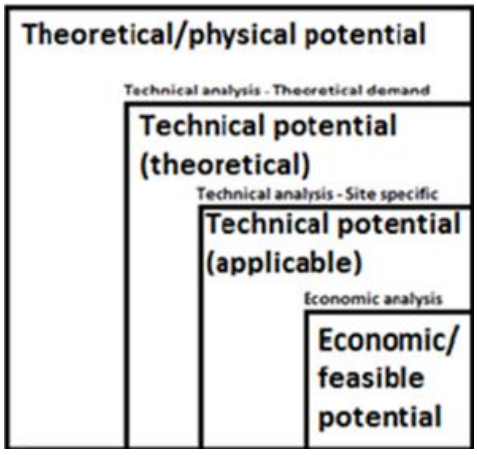

Figure 1.5. Types of Waste Heat Potential Modified [9].

1.2.3. Waste Heat Sources

The main criterion for evaluating the ability of a process to generate useful waste heat or the possibility of using heat as an energy source is the temperature [6]. Generally high temperature waste heat has greater potential for being recovered. However, in certain industries low temperature waste heat is predominant so it is necessary to distinguish between the various levels of temperature of the waste heat to select and optimise the heat recovery technology to be installed. According to S. Brückner *et al.* [6] it is possible to distinguish high temperature waste heat (HT > 400°C), medium temperature waste heat (MT = 100 - 400°C) and low temperature waste heat (LT < 100°C). However, this distinction is not consensual in the literature, with various authors adopting a slightly different classification. Table 1.1 shows the different classifications of residual heat based on the temperature range.

Table 1.1. Different waste heat classifications based on temperature range

Classification 1 [6]**:**	**Classification 2** [10]**:**	**Classification 3** [11]**:**
Low Temperature: < 100°C	Ultra-low Temperature: < 120°C Low Temperature: 120 - 230°C	Low Temperature: < 230°C
Medium Temperature: 100 - 400°C	Medium Temperature: 230 - 650°C	Medium Temperature: 230 - 650°C
High Temperature: > 400°C	High Temperature: 650 - 870°C Ultra-high Temperature: > 870°C	High Temperature: > 650°C

1.2.4. Waste Heat Recovery Technologies

Waste heat recovery is only possible using technologies that capture the heat and transfer it to a gas or liquid that is then used for a certain useful propose that includes fulfilment of new thermal needs, or the generation of mechanical or electrical power [7].

Heat recovery technologies fall into two distinct categories, passive and active (as shown in Figure 1.6). Active technologies increase the temperature of waste heat or transform it into another form of energy. Passive technologies, on the other hand, use heat directly at the same or lower temperature [6].

Active technologies are subdivided into three distinct categories [6], [10].

- Waste Heat to Heat (WHTH) – Waste heat is used to produce thermal energy at a higher temperature. An example of this is the case of heat pumps.
- Waste Heat to Cold (WHTC) – Waste heat is used to produce cooling energy. This is the case for absorption and adsorption chillers.
- Waste Heat to Power (WHTP) - Waste heat is used to produce electricity. This is the case with the organic Rankine and Kalina cycles.

In the case of passive technologies, heat exchangers and thermal energy storage units are the dominant systems.

The choice and application of the recovery technologies depends on each case. Careful assessment is required so that the maximum benefit can be obtained from the residual heat and so that the energy requirements (electrical, mechanical, or thermal) can be met.

Heat pumps are commonly applied to drying processes, air conditioning, distillation, water preheating, washing [12], among others. This type of technology presents high efficiency and an extremely competitive price range when compared to other technologies.

The mechanical vapour compressor or MCV is commonly used in water treatment, desalination, and wastewater treatment [13].

The absorption chiller is a technology applied to several industries namely the petrochemical industry and the paper and cellulose industry [14].

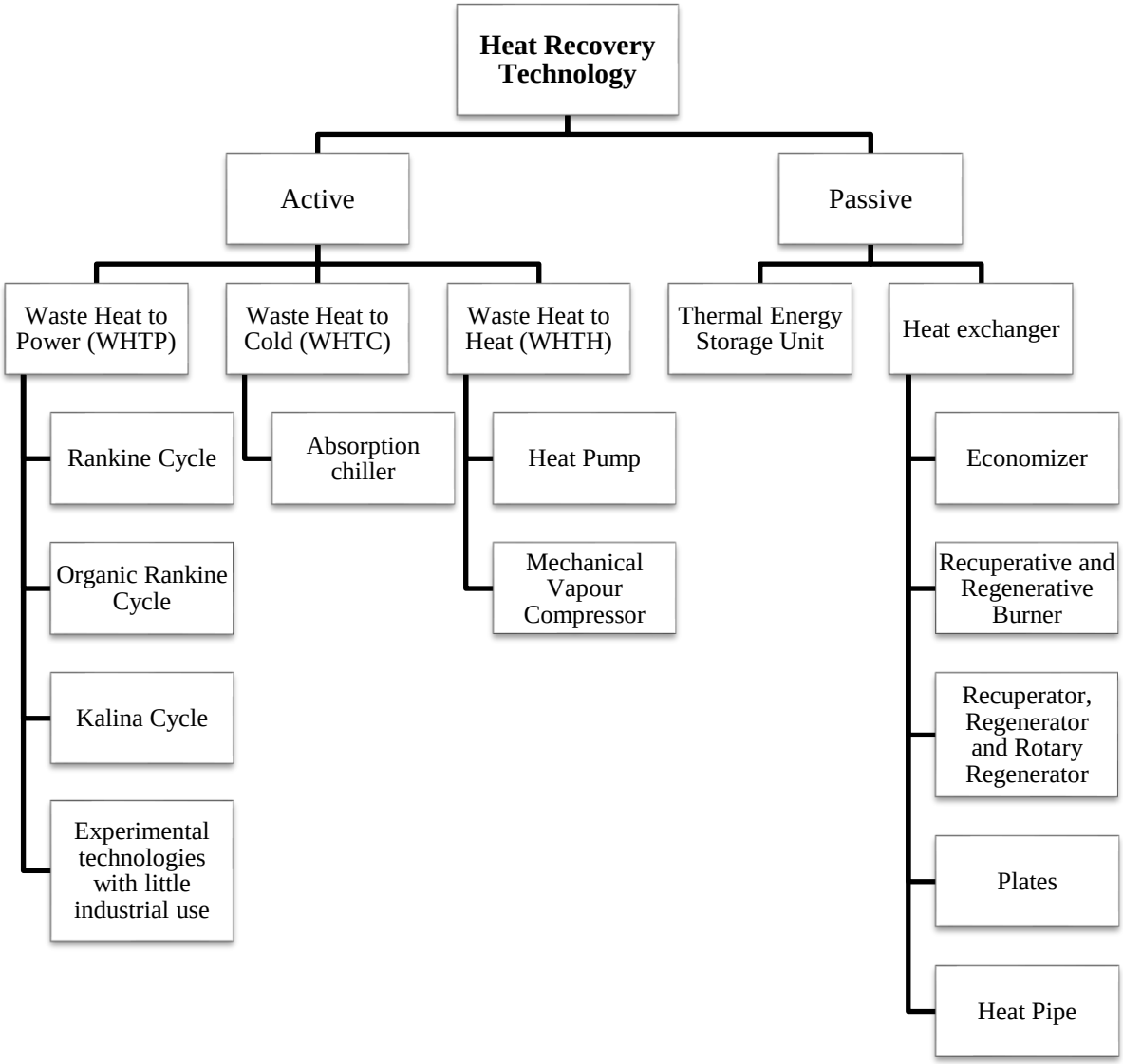

Figure 1.6. Waste Heat Recovery Technologies – Adapted from [6].

The use of economisers is normally associated with the preheating of boiler feed water, allowing an increase in boiler efficiency of around 25 percentual points, reducing fuel consumption. The use of recuperative burners allows an efficiency increase of 30% when compared to conventional burners. Regenerative burners on the other hand allow savings in fuel consumption of between 50 to 60% compared to conventional burners. The thermal wheel is commonly used for heat recovery in AHUs, allowing exhaust heat to be captured and used for heating the new air to be blown in. Heat pipe technology is typically used in furnaces and dryers due to its low maintenance requirements. [12].

Kalina and Organic Rankine Cycles operate at lower temperatures than the typical steam Rankine cycle and are traditionally used in waste heat recover in metalworking industries, in glass and in power generation plants, for mechanical and electrical energy production with energy recuperation rates of 10 and 20% (the Kalina Cycle present slightly bigger efficiency values but with a very small industrial implementation [12]). Other technologies such as the Stirling cycle, the Brayton cycle, thermoelectric generators, and piezoelectric generators are at an embryonic stage of development or are not yet economically viable.

1.3. Organic Rankine Cycle

The Organic Rankine Cycle works on the principle of the traditional Rankine cycle. However, while the traditional Rankine cycle uses water or steam as the working fluid, the ORC uses organic substances (which include carbon compounds) with low boiling points and high vaporization pressures [7]. This feature makes the ORC suitable to operate with different heat sources, such as solar energy, geothermal, biomass/biogas and waste heat [13]. For small powers (up to 10 MW), ORC presents better efficiency and performance than a traditional Rankine cycle.

An ORC typically consists of a pre-heater and an evaporator attached to a heat exchanger, a condenser connected to a recuperator, a pump, and an expansion machine (Figure 1.7).

The heat exchanger is responsible for harvesting the waste heat, heating an intermediate fluid that runs through the evaporator and the pre-heater. The intermediate fluid will be responsible for transferring the energy from the waste heat stream to the organic fluid preheating and vaporising it. The vaporised organic fluid, with high enthalpy and thermal energy, goes through the expansion machine, typically a turbine, expanding. After leaving the expansion machine, the steam passes through the recuperator reducing its temperature and preheating the organic fluid. In the condenser, the steam returns to the liquid state. Finally, in the pump the fluid is pressurized passing again in the recuperator where it is preheated, starting the cycle again [7].

A compilation of some real and theoretical cases of practical application of ORC cycles can be found in ANNEX B.

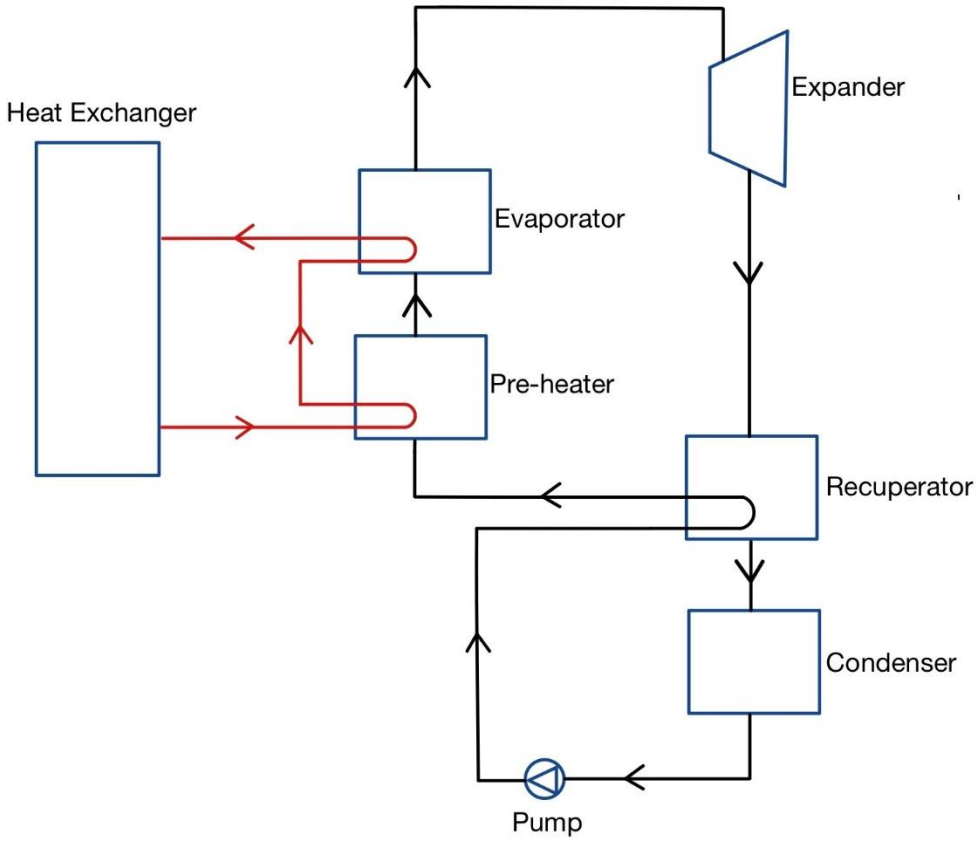

Figure 1.7. Schematic representation of an ORC in a waste heat recovery system.

1.4. Potential for Waste Heat Recovery

The amount of waste heat available varies between the various industry sectors and assumes temperature ranges as wide as [50°C; ≥1000°C] [14]. There is, therefore, a need to evaluate the potential of waste heat by industry sector and by country to analyse the potential implementation of heat recovery systems.

Currently, there are several studies that seek to estimate and quantify the waste heat potential. In general, these studies are based on regional data which are then extrapolated to other areas and countries. It is essential to use the most recent data possible, given the constant evolution of the industrial sector, caused by fluctuations in demand, structural changes, and energy efficiency measures. [14].

Studies such as those presented by M. Papapetrou *et al.* [14], by G. Bianchi *et al.* [15] and G. P. Panayiotou *et al*. [9] develop a waste heat analysis methodology that is specific to each industrial sector and to each EU country. The result of these studies is a complete

mapping of the residual heat potential [14]. The study conducted by C. Forman *et al.* [16] presents more generalised data than the previous ones.

The methods used in each study will be presented together with an evaluation of the results obtained. Finally, a brief comparison between results will be made.

1.4.1. Industrial waste heat: Estimation of the technically available resource in the EU [14]

1.4.1.1. Methodology

In the study developed by M. Papapetrou *et al.* [14] the study developed by G. P. Hammond *et al.* [17] is used as a starting point, which uses waste heat data from 425 industries in the UK in the period 2000-2003. The use of such many industries strength the confidence in the results obtained [17].

The first step of the methodology followed by C. Forman *et al.* [16] is the calculation of the waste heat fraction (WHF) for each temperature range and industrial sector, using the data obtained by U. Persson *et al.* [18] and Equation (1.1).

$$\left(WHF_{UK,sector,Temp\ Range}\right)_{2000-2003} = \left(\frac{(waste\ heat\ potencial)_{UK,sector,Temp\ Range}}{(heat\ consumption)_{UK,sector}}\right)_{2000-2003} \quad (1.1)$$

The second step consists in adapting the set of WHF's, calculated in the previous step, for each reality of the remaining EU countries. For that, in Equation (1.2), the WHF's for the UK sector is multiplied by a factor $(EI_{EU\ country,sector}/EI_{UK,sector})$ that relates the energy intensity of each country in comparison with the UK.

$$\left(WHF_{EU,sector,Temp\ Range}\right)_{2000-2003} = \left(WHF_{UK,sector,Temp\ Range}\right)_{2000-2003}\left(\frac{EI_{EU\ country,sector}}{EI_{UK,sector}}\right) \quad (1.2)$$

In the third step it is necessary to update the previously calculated values, to consider, the developments in energy efficiency and the evolution of industrial sectors in the year under analysis. For this purpose, in Equation (1.3), the result obtained in Equation (1.2) is multiplied by a factor $\left(\left(EI_{EU\ country,sector}\right)_{Year}/\left(EI_{EU\ country,sector}\right)_{2000-2003}\right)$ that represents the ratio of the energy intensity values between the year of analysis and the values

obtained in the period 2000 - 2003. In the case of this study the data used refers to the year 2015.

$$\left(WHF_{EU,sector,Temp\ Range}\right)_{Year} = \left(WHF_{EU,sector,Temp\ Range}\right)_{2000-2003} \frac{\left(EI_{EU\ country,sector}\right)_{Year}}{\left(EI_{EU\ country,sector}\right)_{2000-2003}} \quad (1.3)$$

The fourth and last step, consists in the multiplication of the heat consumption, obtained using Eurostat data, for the year in analysis and for each industry, by the values obtained using Equation (1.3). Thus, it is possible to obtain an estimate for the year under analysis, avoiding large uncertainties associated with the differences in energy efficiency of each country and between different years [14].

1.4.1.2. Results

In the study developed by M. Papapetrou *et al.* [14] the industrial sectors are divided into 6 distinct categories: Iron & Steel; Non-ferrous metal; Chemical; Non-metallic mineral; Food, drink & tobacco; Paper & pulp; Other industries.

According to the results obtained in the study developed by M. Papapetrou *et al.* [14] for the year 2015, the theoretical technical potential of EU waste heat is estimated at 304.13 TWh/year. As is visible in Figure 1.8, a large part of this potential lies in the 100-200°C range, about 100 TWh/year, with waste heat below 100°C presenting an almost negligible potential (1.25 TWh/year). The range 200-500°C presents a potential of about 78 TWh/year, while for temperatures above 500°C a potential of about 124 TWh/year is presented.

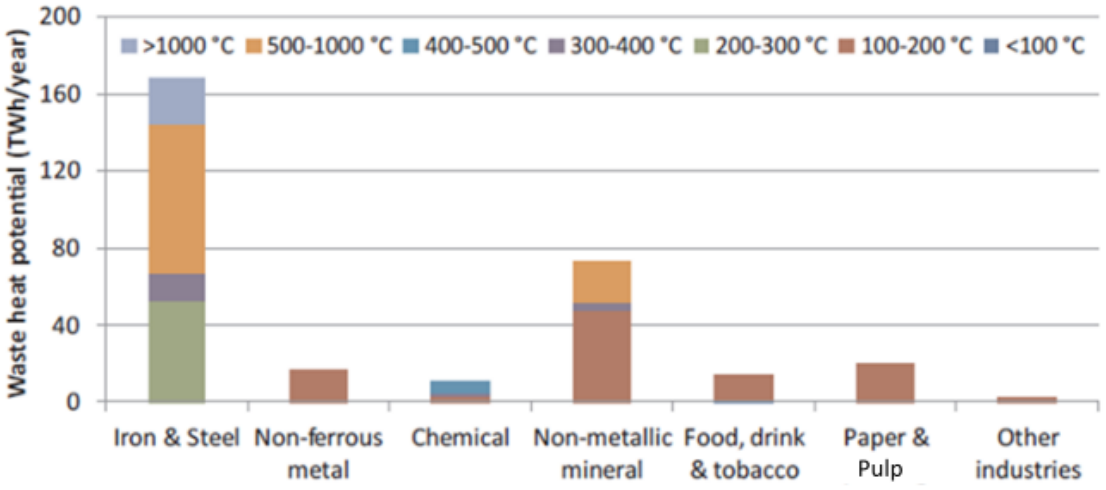

Figure 1.8. Theoretical technical potential by industry sector and temperature level in the EU [14].

From Figure 1.8 it can be concluded that the heat potential above 500°C is limited and only available in the non-metallic minerals industries (for example the cement industry [14]) and the steel and iron industry. For temperatures between 200 and 500°C the range of industries where such heat streams is available increases, with the steel and iron industry remaining an integral part but being accompanied by the pulp and paper industry. Most of the waste heat potential lies between 100 and 200°C and is found in virtually all industries. Finally, the waste heat potential for temperatures below 100°C is very low when compared to the other temperature levels and only exists in the food and tobacco industry for preheating and drying processes. The reasons for this are: very low temperature difference compared to ambient temperature, very low heat consumption within this range and very low heat losses [14].

As it was expected, most of the theoretical technical waste heat potential lies in only 5 countries, the United Kingdom, Germany, Italy, Spain, and France. Together these countries account for 60% of this potential.

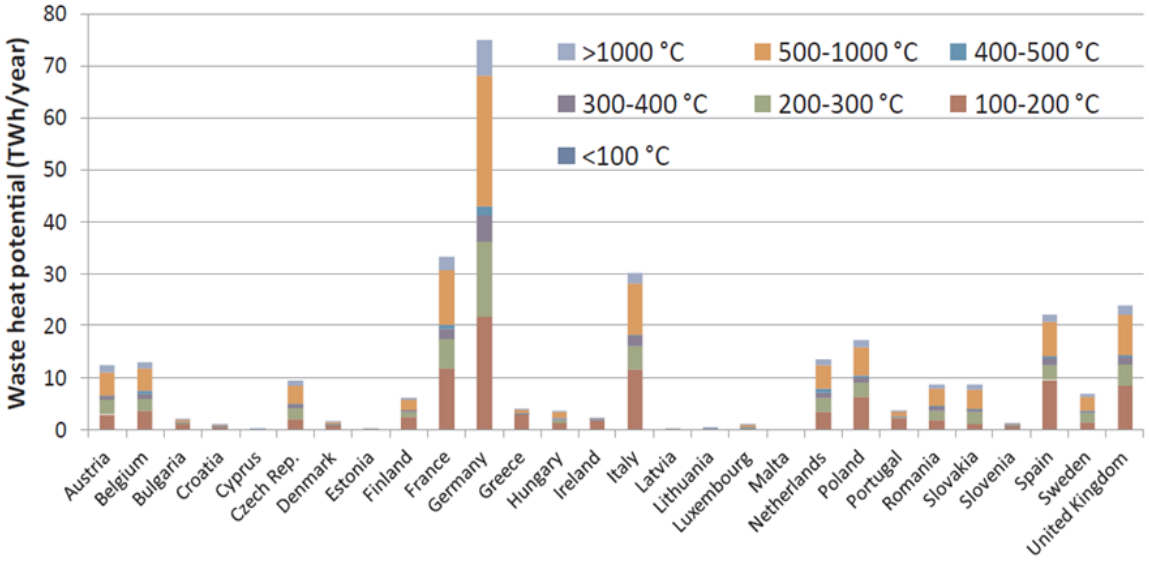

Figure 1.9. Theoretical Technical Potential for each EU country, by temperature for all industries - Adapted from [14].

Most EU countries have a mix of different industries, however, as can be seen in Figure 1.9, some have only one dominant industry with negligible potential within the EU.

1.4.2. Estimating the waste heat recovery in the European Union Industry [15]

1.4.2.1. Methodology

The study developed by G. Bianchi *et al.* [15] goes one step further and there is a separation between theoretical technical potential and Carnot potential of the waste heat. The Carnot potential refers only to the heat that can be used to produce electricity. Using the methodology followed in this study, the Carnot potential will be estimated, serving as a starting point the theoretical/ thermodynamic potential of the waste heat.

To calculate the theoretical potential, and following the symbology adopted in the study developed by G. Bianchi *et al* [15], we resort to Equation (1.4):

$$WHRP = \sum_{i=1}^{N}\sum_{j=1}^{M} \lambda_{ij} E_{ij} \tag{1.4}$$

Where E_{ij} is the primary energy consumption from a given source and λ_{ij} the percentage of primary energy from a process that is lost by waste heat. In this last term (λ_{ij}) only the heat lost in the form of exhaust gases and effluents (such as water or cooling air) is accounted for. Excluded from the calculation are heat losses by radiation, friction, and electrical transmission [15].

Using Equation (1.5) it is possible to arrange the theoretical potential according to temperature. For this, the classification considered is low temperature heat < 100°C, medium temperature 100 - 300°C and high temperature > 300°C.

$$WHRP = \sum_{i=1}^{N}\sum_{j=1}^{M}\sum_{k=1}^{3} \sigma_{ijk} \lambda_{ij} E_{ij} \tag{1.5}$$

With σ_{ij} incorporating the weight of each industry with a sum equal to 1. The k-sub-script referring to the temperature levels: k=1 for low temperature, k=2 for medium temperature and k=3 for high temperature.

From a thermodynamic point of view the energy corresponds to the sum of the exergy with anergy. While exergy corresponds to the energy that can be transformed into work, anergy represents the exergy that is destroyed. So, to estimate the amount of exergy present in the waste heat we resort to Carnot's theorem. According to this theorem the maximum

thermal efficiency of a thermal machine is determined by the thermal characteristics of the two thermal reservoirs [15].

That said, in Equation (1.6), to obtain the Carnot potential, a Carnot efficiency coefficient (η_C) is applied to the residual heat obtained and the corresponding temperature ranges.

$$CWHRP = WHRP \times \eta_C = WHRP \times \left(1 - \frac{T_c}{T_h}\right) \quad (1.6)$$

1.4.2.2. Results

In the study developed by G. Bianchi *et al.* [15], the Carnot potential is only 279 TWh/year, lower than the 304.13 TWh/year calculated by the study developed by M. Papapetrou *et al.* [14] for the theoretical technical potential. According to the theoretical potential, the dominant waste heat would be that of low temperature (<100°C), however due to its low exergy, it is possible to conclude that the Carnot potential is mainly at temperatures above 300°C, with the medium temperature waste heat (100 - 300°C) also presenting an important share (Figure 1.10 (b)).

As is visible in Figure 1.10 (a), as in the study conducted by M. Papapetrou *et al.* [14], the steel and iron industry remain predominant, with 54.3 TWh/year of the Carnot potential of waste heat. It is closely followed by the non-metallic minerals industry (43.8 TWh/year), the food and tobacco industry (35.1 TWh/year), the chemical industry (33.9 TWh/year) and the pulp and paper industry (27.0 TWh/year). Other unspecified industries (19.9 TWh/year), machinery industries (19.6 TWh/year) and non-ferrous metals (14.1 TWh/year) also present relevant potential values.

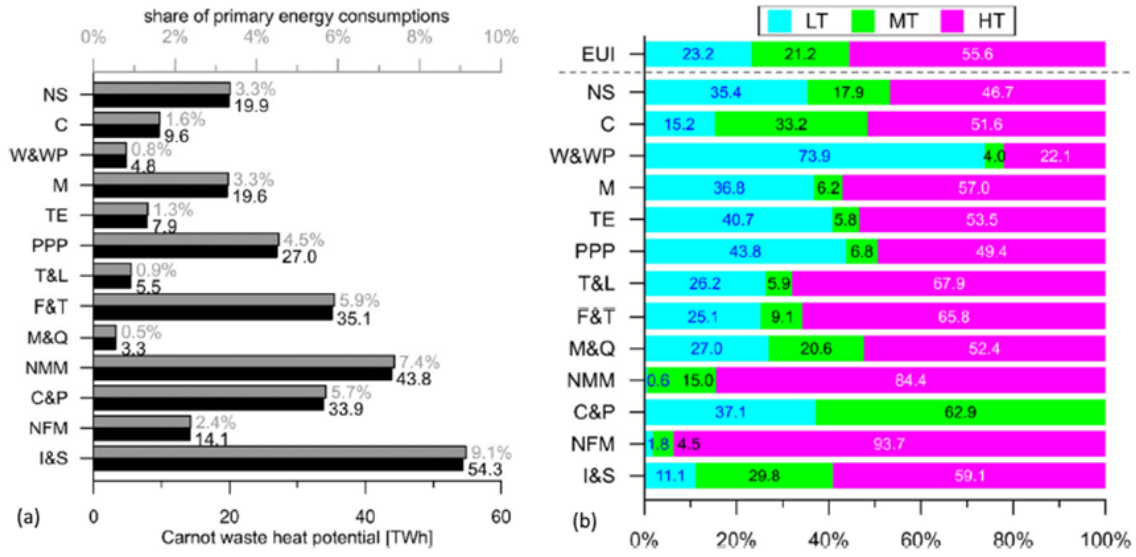

Figure 1.10. (a) - Carnot potential of waste heat and relevance in primary energy consumption for EU industries; (b) - Carnot potential of waste heat distributed by waste heat classification for EU industries. - Adapted from [15]. With: NS – Non-specified (industry); C – Construction; W&WP – Wood and wood products; M – Machinery; TE – Transport equipment; PPP – Paper, pulp, and print; T&L – Textile and leather; F&T – Food and tobacco; M&Q – Mining and quarrying; NMM – Non-metallic minerals; C&P – Chemical and petrochemical; NFM – Non-ferrous metal; I&S – Iron & Steel

Looking at Figure 1.11, it can be concluded that Germany, France, Italy, the United Kingdom, and Spain continue to be the countries with the greatest potential for waste heat utilisation.

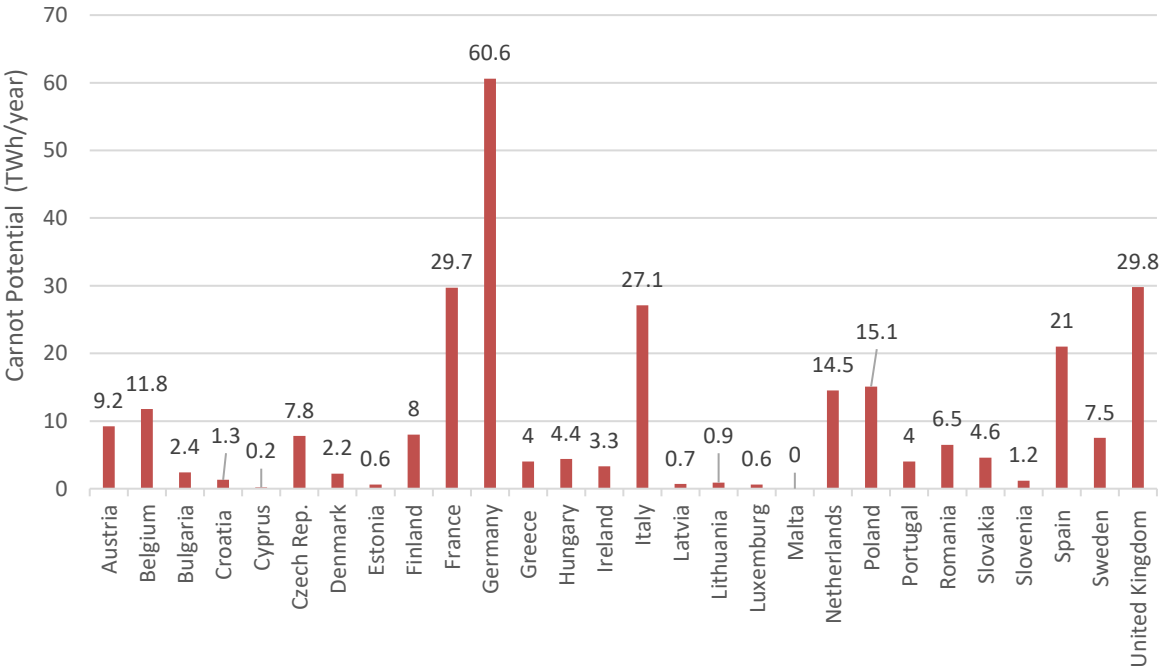

Figure 1.11. Carnot Potential of Waste Heat for different EU countries [15]

1.4.3. Estimating the global waste heat potential [16]

1.4.3.1. Methodology

The methodology used in this study is quite different from the previous ones, being based on a top-down approach, where general results are used to obtain the waste heat fluxes associated to each process [8], [16].

To calculate the theoretical potential of waste heat, this study takes as its initial basis the estimate of energy flows, conducted by the IEA (International Energy Agency), which covers the entire energy chain, from primary energy consumption to final energy use by sector.

The second step of this methodology consists in determining the energy balances that occur in each sector and in each process. The great challenge consists in obtaining a scientifically acceptable compromise, for the input parameters, between the global evaluation as a whole and for each process. This challenge occurs due to the difficulty in defining the global energy flow, where data is not available, depending on a survey of literature to obtain these values. The challenge is solved considering the investigations conducted by J. M. Cullen *et al.* [19] and the data that was obtained from the study developed by N. Nakićenović *et al.* [20].

After collecting the data, it is necessary to associate the processes and equipment used in each sector with the respective fuel (input) used (coal, natural gas, petroleum products, electricity, heat, among others). For this we again resort to IEA's statistical data. Based on balance coefficients (η_{ES}, η_{EL} e η_{OL}) which depend on the processes and equipment (Equation (1.7)), the energy output can be interpreted as the sum between energy losses and the final use of energy (Figure 1.12), whether for heat production, electricity, or movement.

$$\eta_i = \frac{Energy\ Output\ (Flow)}{Energy\ Input\ (Process)} \tag{1.7}$$

In this study, waste heat appears in losses, which are divided into three distinct categories: exhaust gas losses; effluent losses; other losses. Only the waste heat associated with exhaust and effluent losses is considered in this study. Radiation, transmission, friction, conduction, convection, and electrical resistance losses are excluded.

As in the study developed by G. Bianchi *et al.* [15], there is separation between theoretical potential and Carnot potential of the waste heat. Thus, it is used Equation (1.6) to obtain the Carnot potential.

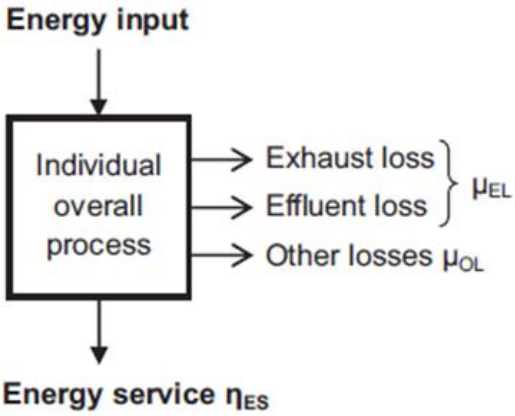

Figure 1.12. Energy balance associated to the process - Adapted from [16].

1.4.3.2. Results

Contrary to the studies developed by M. Papapetrou *et al.* [14] and by G. Bianchi *et al.* [15], the methodology adopted provides less detailed results, dividing the potential by more generalized sectors, not performing an industry assessment, as would be ideal.

From the analysis of the results (Figure 1.13 and Figure 1.14) it is observable, for the theoretical potential in the world, that 63% of the waste heat is obtained at temperatures below 100°C, 16% between 100 and 299°C and 21% at temperatures above 300°C. However, when analysing the Carnot potential, the perspective changes, with only 21% of the Carnot potential occurring for temperatures below 100°C, 24% for temperatures between 100 and 299°C and 55% for temperatures above 300°C.

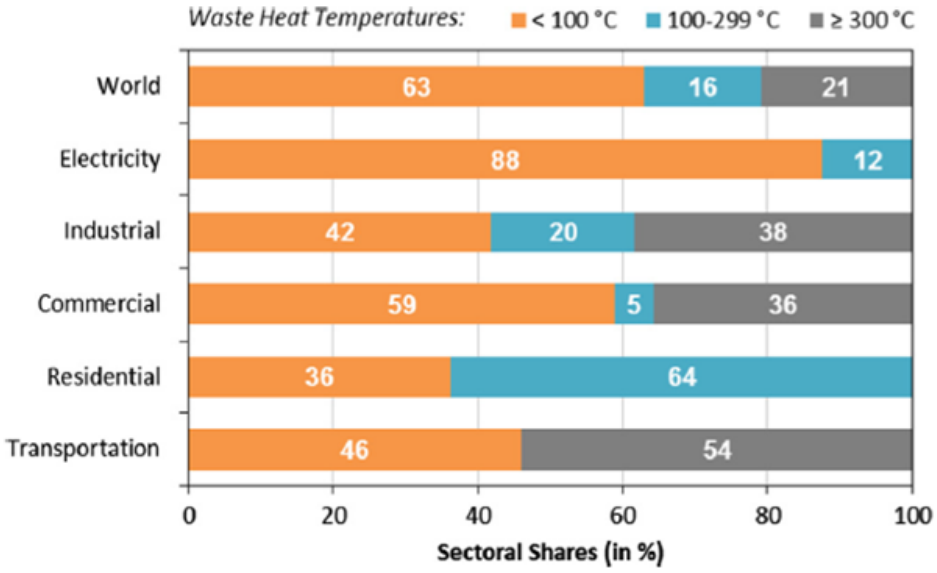

Figure 1.13. Theoretical waste heat potential distribution by sector and temperature range - Adapted from [16].

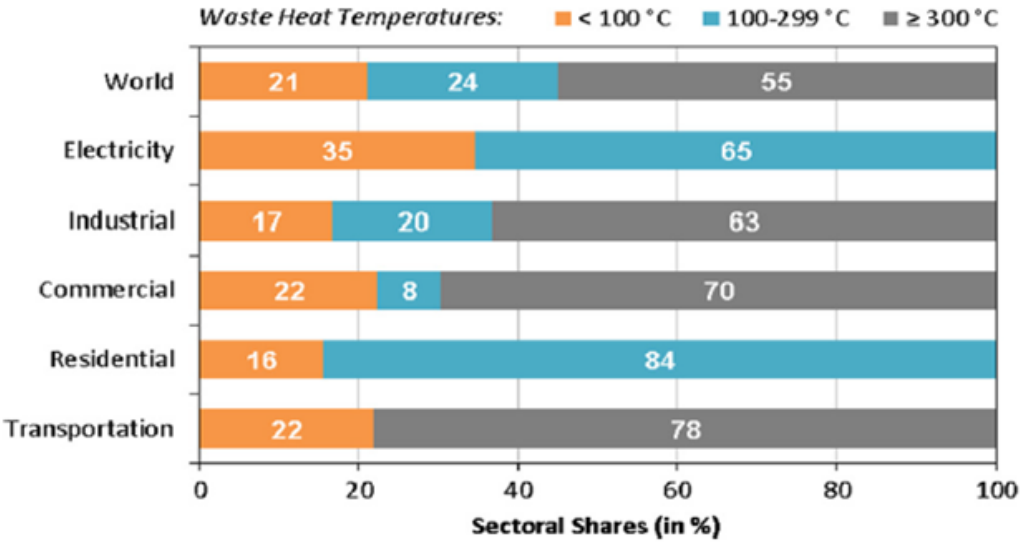

Figure 1.14. Carnot Potential distribution of waste heat by sector and temperature range – Adapted from [16].

Looking at Figure 1.15, according to this study, 25% of the Carnot potential is linked to the commercial sector, 22% to the residential sector, 34% to industry, 35% to transport and 5% to electricity generation.

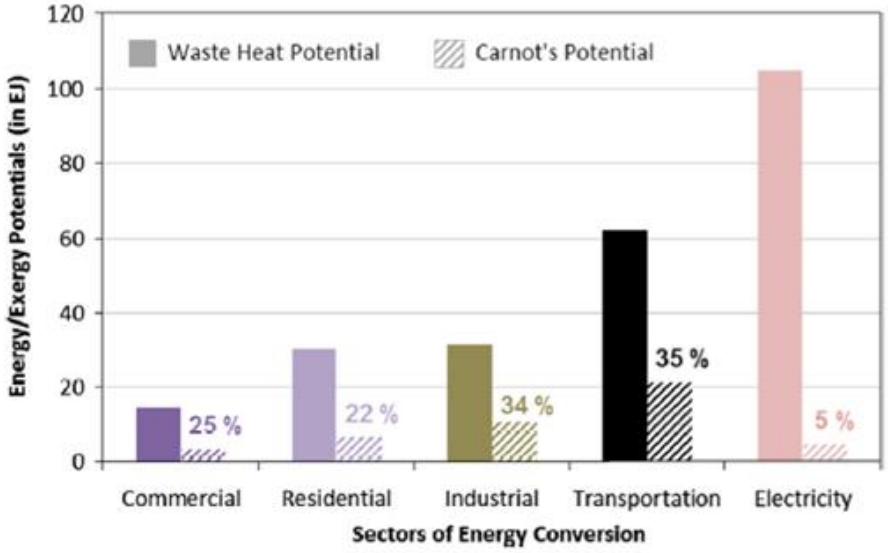

Figure 1.15. Theoretical and Carnot potential distribution by sector - Adapted from [16].

1.4.4. Preliminary assessment of waste heat potential in major European industries [9]

1.4.4.1. Methodology

To draw conclusions on the potential of waste heat, this study uses statistical data on the energy consumption of the industrial sector of each EU country, combining this data with the factors used in the study developed by C. Forman *et al.* [16]. This translates into more detailed results per industry and country.

1.4.4.2. Results

Performing an analysis of the theoretical waste heat potential (Figure 1.16) it is observable that industries such as steel and iron (22%), chemical and petrochemical (22%) and non-metallic minerals (14%) are dominant. This is followed by the pulp and paper industry (13%), unspecified industries (13%), food and tobacco industry (9%), non-ferrous metals industry (3%), wood industry (2%) and textile industry (2%).

When analysing the Carnot potential (Figure 1.17), the paradigm changes a lot, with the steel and iron industry accounting for 27% of this potential. The chemical and petrochemical industry follows with 22%, the non-metallic minerals industry with 17%, the pulp and paper industry with 12%, unspecified industries with 12%, the food and tobacco industry and the non-ferrous metals industry both with 4%, wood with 1% and finally the textile industry also with 4%.

It is apparent that the percentage of theoretical potential and the percentage of Carnot potential can vary from industry to industry. This is due to the different temperature ranges typical of each industry. If an industry uses mostly high temperature processes, the Carnot potential will be higher than the theoretical potential in percentage, if it uses mostly low temperature processes, the opposite happens.

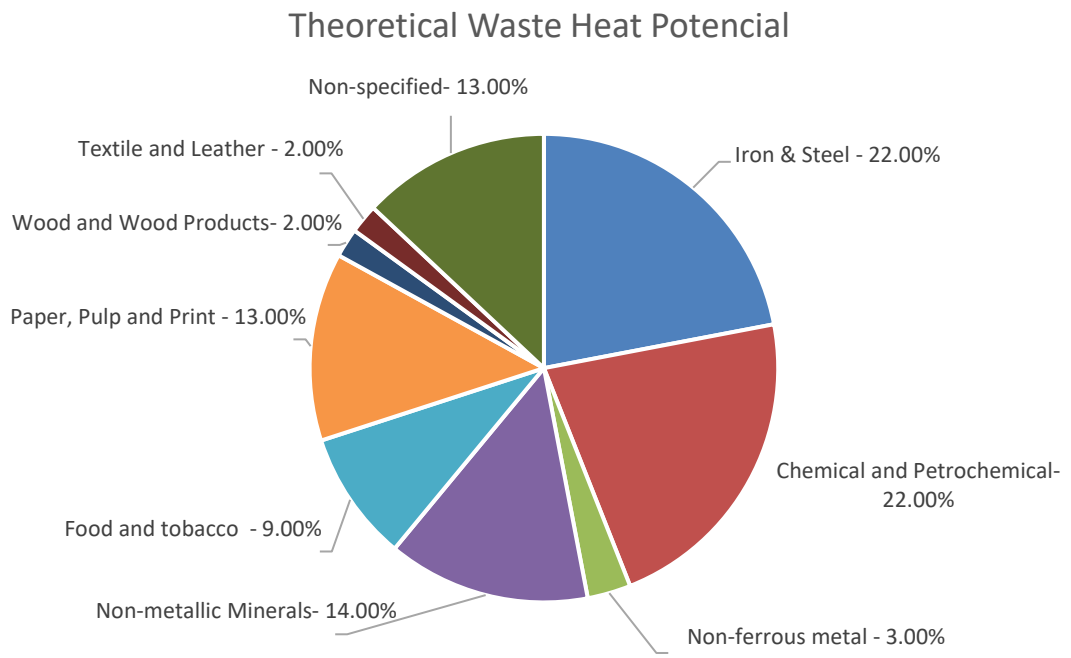

Figure 1.16. Theoretical Waste Heat Potential – Adapted from [9].

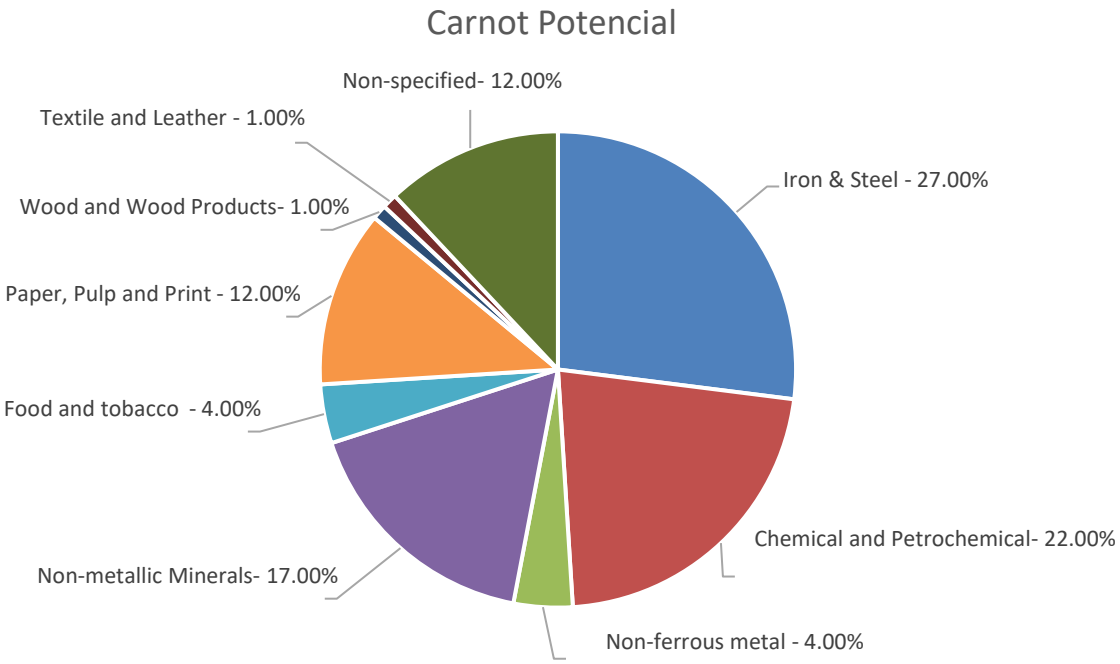

Figure 1.17. Carnot Potential of Waste Heat - Adapted from [9].

As expected, the global values of theoretical potential and Carnot potential are different from the studies developed by M. Papapetrou *et al.* [14] and by G. Bianchi *et al.* [15]. According to this study the theoretical potential is 370.41 TWh/year, with the Carnot potential of only 173.99 TWh/year.

What remains, however, is the dominance of German, French, Italian, Spanish and UK industries (Figure 1.18).

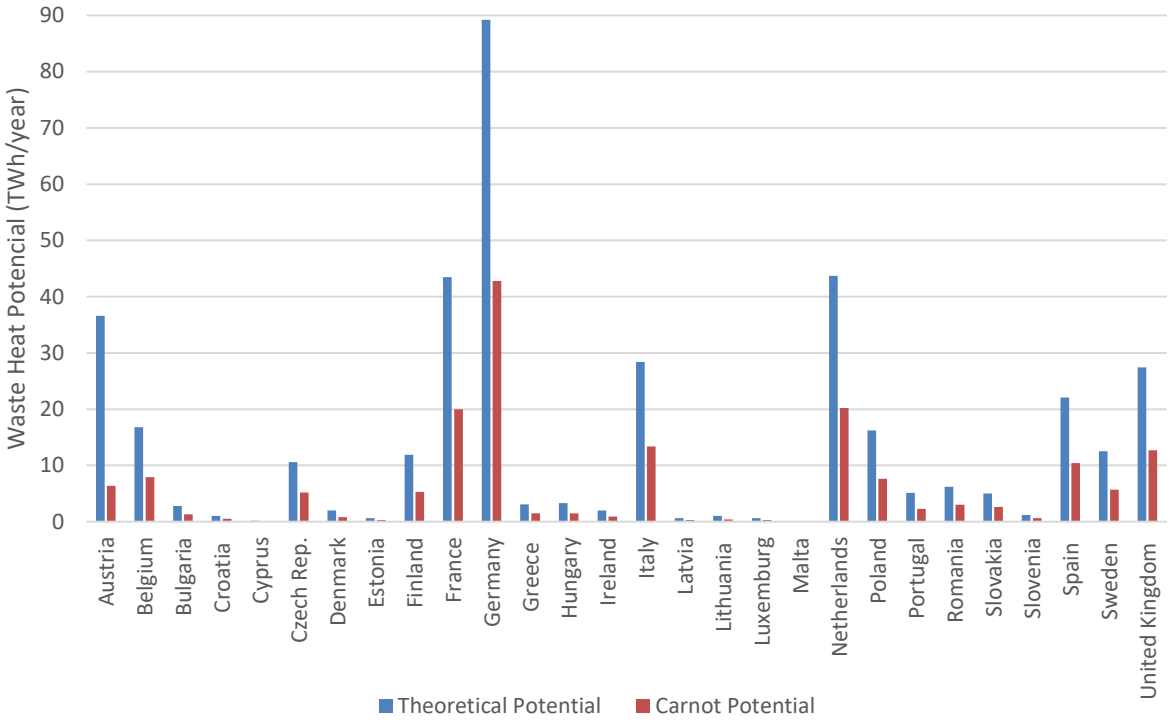

Figure 1.18. Theoretical and Carnot potential of waste heat for different EU countries - Adapted from [9].

1.4.5. Thermal Energy Harvesting [21]

Based on previous studies developed by C. Forman *et al.* [16], by U. Persson *et al.* [18] and by X. Jeroen de Beer *et al.* [22] in the study developed by M. Astolfi *et al.* [21] a compilation of waste heat by temperature and its quantity by industrial sector is made (Figure 1.19).

A survey of industrial areas with significant waste heat potential and their location is also conducted (see Figure 1.20).

	Temperature range of waste thermal energy / °C								
	<100	100 – 200	200 – 300	300 – 400	400 – 500	500 – 600	600 – 1000	>1000	TWh/a
Iron and Steel									73.0
Non-metallic minerals									91.2
Clinker*									
Glass*									
Non ferrous metals (Primary aluminum*)									32.3
Chemical and Petrochemical									141.7
Pulp, Paper and Printing*									125.5
Others									263.0
Refinery*									
Food and Beverages									115.2
Gas and Diesel Engines									2013.5

Figure 1.19. Waste heat distribution by temperature and industry and its quantification. Fraction of waste heat per temperature range indicated by blue squares with light blue <20%, normal blue <50%, dark blue >50%. - Adapted from [21].

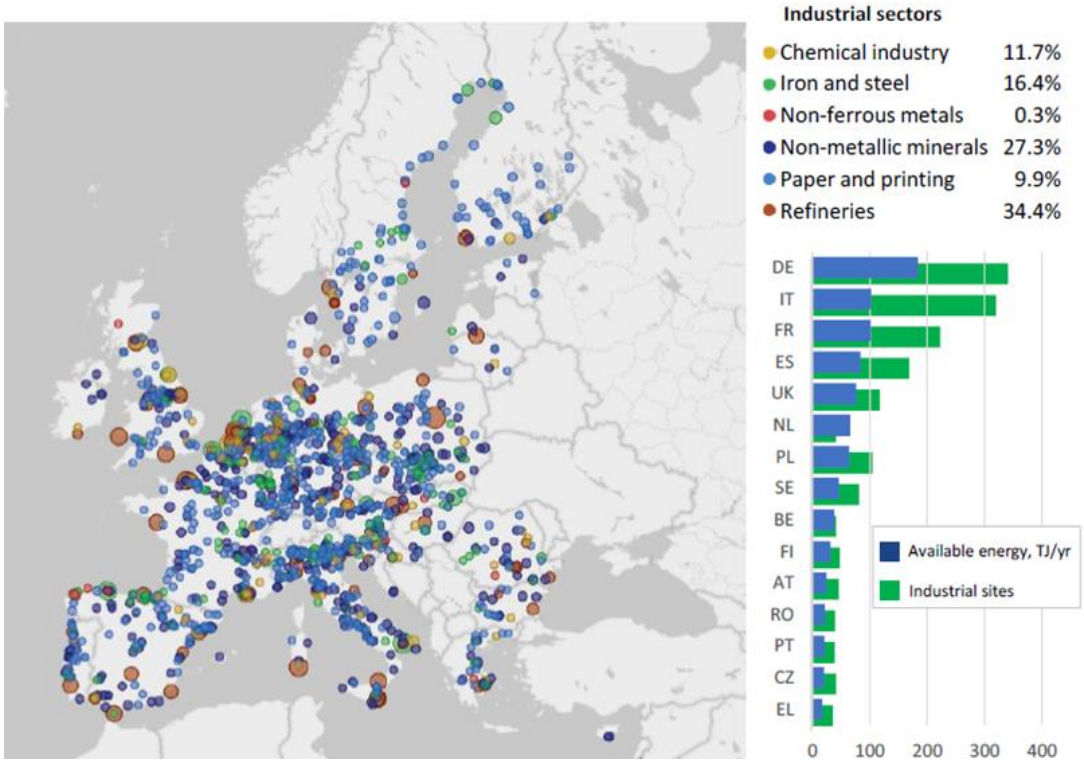

Figure 1.20. Map of industrial sites with waste heat potential in Europe - Adapted from [21].

As it could be expected, from the analysis of Figure 1.20 it can be concluded that countries like Germany, Italy, France, Spain, and United Kingdom present the largest values of waste heat, having a direct relation with the largest number of industries.

Finally, in Table 1.2, it is conducted an evaluation of the theoretical potential and the Carnot potential in the industry through ORC power plants, obtaining the values of 882 TWh/year for the theoretical potential and 150 TWh/year for the Carnot potential. Note that according to this study the highest values of potential occur in the temperature range 200 - 500°C.

Table 1.2. Theoretical Potential and Carnot Potential according to temperature ranges for Europe - Adapted from [21]

Temperature range [°C]	Theoretical Potential [TWh/year]	Carnot Potential [TWh/year]	Installable Capacity [GW_{el}]
< 100	390.4	32.2	4.0
100 - 200	60.5	2.8	0.3
200 - 500	334.7	68.5	8.6
> 500	97.2	47.2	5.9
Total	**882.8**	**150.7**	**18.8**

1.4.6. Study Comparison

A brief comparison between the methods analysed (ANNEX C) reveals a clear qualitative convergence between results, both between industries and countries. However, there is no quantitative convergence, as it was already expected, due to the difference among the methodologies used. By using a Carnot efficiency, the residual heat calculation is restricted to what can be used to produce electricity. This makes the values of the potential use of waste heat underestimated, since the waste heat that can be used for heat production, cooling or passive use is not considered (Figure 1.6).

The study performed by G. Bianchi *et al.* [15] is much more conservative and quantitatively underestimated than the study performed by M. Papapetrou *et al.* [14]. The method used by G. P. Panayiotou *et al*. [9] is less precise and the method presented by C. Forman *et al.* [16] is less detailed than those followed by M. Papapetrou *et al.* [14] and by G. Bianchi *et al*. [15]. The study performed by M. Astolfi *et al.* [21] presents itself as being the most recent, however lacks the detail found in other studies.

In ANNEX D, it can be found a compilation of typical industrial processes and temperatures.

2. CONCEPTUALISATION OF A TEST STAND

The SCIVEN company is responsible for the development, albeit in an embryonic state, of a modulating product that recycles waste heat in electricity production. At the current stage of product development, it is justified to design a test bench to simulate several typical industrial conditions. The objective of this test stand is to be able to produce different waste heat streams at different temperatures.

This test rig will consist of a natural gas burner, a combustion and mixing chamber and of a heat exchanger responsible for transferring the heat from the combustion products to an organic fluid operating according to an ORC (SCIVEN's modulating product).

The natural gas burner and the combustion and mixing chamber are designed to obtain various waste heat streams typical in industry, with the possibility of varying their outlet power and temperature.

The heat exchanger will capture the power of the heat streams and transfer it to an intermediate thermal oil.

The development will be done in three steps. The first phase of the development consists of dimensioning the natural gas line that will feed the burner.

The second stage will involve selecting a burner, dimensioning the combustion, and mixing chamber.

The third step consist in the design and optimization of a heat exchanger and its parametric analysis. A conceptual 3D model of the test stand will be presented.

2.1. Natural Gas Supply Line

Typically, when there is a change in the needs for natural gas, i.e., when the number of equipment consuming this fuel changes, the whole installation is sized/resized. It would then be necessary to resize the RMP (Regulation and Measurement Post) which is supplied by a primary natural gas network installed on public road. Also downstream of the RMP it would be necessary to re-dimension the interior distribution network that supplies the equipment [23].

However, the only change to be made will be the installation of a burner with a maximum power of approximately 200 kW. Since it is assumed that the natural gas consuming equipment present in the building will never be operating simultaneously, the solution of using a bifurcation of a pre-existing 3-inch supply pipe will be implemented. A pipe will thus be sized derived from this bifurcation which will serve to transport the natural gas responsible for feeding the burner. The pipe length will be approximately 50 metres.

The sizing of this pipe will be conducted using 2 different methods. The first method follows the methodology adopted by APTA *(Associação de Produtores de Tubos em Aço soldados longitudinalmente e acessórios em ferro Fundido maleável roscados para canalizações).* The second method is more traditional and uses the equation of conservation of energy of a particle along a path to obtain the pressure drop along the pipe.

In both methods it is necessary to ensure that two conditions are met to avoid vibrations or noise normally associated with high speed. These conditions can be found in *Decreto-Lei nº 292/2000*, for low pressure installations: Pressure drop in the pipe section < 1.5 mbar; Flow velocity < 10 m/s.

2.1.1. First Method

The 1st method adopted is the one followed by APTA [24]. All the following equations follow the model adopted by APTA [24].

First, the feed rate required for the burner must be calculated:

$$Q_{Burner}\left[\frac{m^3}{h}\right] = 860\left[\frac{Kcal}{kWh}\right] \cdot \frac{P_{nom}\,[kW]}{LHV\,\left[\frac{kcal}{m^3}\right]} \cdot \frac{T_{st}[K]}{T_n[K]} \tag{2.1}$$

With P_{nom} corresponding to the nominal power of the burner, LHV to the lower heating value of natural gas, T_{st} to the absolute standard temperature (288.15 K) and T_n to the absolute normal temperature (273.15 K).

$\frac{T_{st}}{T_n} = \frac{288.15}{273.15} = 1.055$, and $LHV = 10.718217\,[\frac{kWh}{m^3}]$ → Obtained from https://www.ign.ren.pt/.

The 2nd stage is to calculate the diameter of the pipe, following Equation (2.2), that is an adaptation of the Renouard formula.

$$D_{calculation} = [(22750 \cdot d_c \cdot Q_{section}^{1.82})/J]^{1/4.82} \tag{2.2}$$

With:

- 22750 → Empirical constant adapted from the Renouard formula [25]
- Natural Gas corrected relative density: $d_c = 0.62$ → measured in relation to dry air at a temperature of 20°C and an absolute pressure of 101.325 kPa;
- $Q_{section}[m^3/h] = Q_{Burner}[m^3/h]$;
- Average linear pressure drop [mbar/m]: $J = \Delta P_{adm}/L_{eq.max}$;
- $\Delta P_{adm} = 1.5\ mbar$ → Maximum allowable pressure variation in accordance with *Decreto-Lei nº 292/2000*;
- $L_{eq.max} = 1.2 \cdot L_{critical}$ → 20% increase that provides extra security;
- $L_{critical}$ = 50 m → sum of the lengths of the different sections of pipe that make up the critical path (longest length of pipe, which in this case corresponds to 50 m).

After obtaining $D_{calculation}$ it is necessary to normalise the value obtained to the nearest upper diameter, in accordance with EN 10255.

The last stage of this methodology involves calculating the value of the pressure drop along the pipe and the flow velocity and comparing both with the criteria to be met.

The final pressure, P_f, in the section is obtained using adapted Renouard formula (APTA) for low pressure (Equation (2.3)):

$$P_f = P_i - 22750 \cdot d_c \cdot L_{eq} \cdot \frac{Q_{section}^{1.82}}{D_i^{4.82}} \quad (2.3)$$

For the calculation of the corrected final pressure in the section P_{fc}, which incorporates the static pressure drop (Equation (2.4)) :

$$P_{fc} = P_f + 0.1202 \cdot (1 - d_r) \cdot h \quad (2.4)$$

With:

- $L_{eq} = L_{eq.max} + L_{eq,local}$;
- $L_{eq,local} = \sum Local\ pressure\ drops\ using\ equivalent\ lengths\ method$
- Natural Gas relative density $d_r = 0.65$;
- Difference in elevation between the beginning and the end of the section $h = -1.5\ m$;
- $P_i = 20\ mbar$ → initial pressure of each section;

- $D_i =$ Normalised diameter

Finally, the cumulative head loss in the section under study will be given by Equation (2.5):

$$\Delta P_{Total} = P_i - P_{fc} \tag{2.5}$$

If $\Delta P_{Total} < 1.5$ mbar the criterion is fulfilled.

To calculate the flow velocity, Equation (2.6) is followed:

$$v = 354 \cdot (Q_{section} \cdot P_0)/(D_i^2 \cdot P_m) \tag{2.6}$$

With:

- $P_m = \frac{P_i + P_{fc}}{2} + P_0 \rightarrow$ average pressure in each section;
- $P_0 = P_{atm} = 1013.25\ mbar$.

If $v < 10$ m/s the criterion is fulfilled.

In the current case using the using the equivalent lengths method, and considering 4 local head losses (4 x 90° sharp bends) with a value of 0.67 [m] each, the values obtained according to this method are:

- $D_i = 53.1\ mm = \ 2\ inches$;
- $\Delta P_{Total} = 0.88\ mbar < 1.5\ mbar$;
- $v = 2.42\ m/s < 10\ m/s$.

It can therefore be concluded that the standard diameter DN50 meets the required criteria.

2.1.2. Second Method

The 2nd method uses a traditional approach, starting from the equation of conservation of energy of a particle (Equation (2.7)):

$$\left(\frac{P_i}{\rho g} + \frac{{v_i}^2}{2g} + z_i\right) = \left(\frac{P_f}{\rho g} + \frac{{v_f}^2}{2g} + z_f\right) + (f \times \frac{L}{D} + K_i) \times \frac{v^2}{2g} \tag{2.7}$$

With:

- $v_i = v_f\ m/s$; $v_i \rightarrow$ particle speed at the starting point; $v_f \rightarrow$ particle speed at the end point.
- $z_i = 0\ m \rightarrow$ elevation at the starting point;
- $D = \ D_i = 53.1\ mm \rightarrow$ impose, to verify that it meets the criteria;

- $L = L_{eq} \rightarrow$ using the equivalent lengths method;
- $K_i = 0 \rightarrow$ as the method of equivalent lengths is used; K_i is an empirical dimensionless factor that predicts local losses.
- $f = \begin{cases} \frac{64}{Re_d}, Re_d < 2300 \\ \left\{-1.8log_{10}\left[\frac{6.9}{Re_d} + \left(\frac{\varepsilon/D_i}{3.7}\right)^{1.11}\right]\right\}^{-2}, Re_d > 2300 \end{cases}$;
- $Re_d = \frac{\rho \times v \times D_{eq}}{\mu} = \frac{v \times D_{eq}}{\nu}$;
- $\varepsilon = 0.0006 \rightarrow$ steel pipe roughness factor;
- $v\,[m/s] = Q[\frac{m^3}{s}]/A[m^2] = 4Q/(\pi \cdot {D_i}^2)$.

Taking the previous values into account, Equation (2.7) takes the form of Equation (2.8):

$$P_i - P_f = \Delta P_{Total} = \left(f \times \frac{L}{D} \times \frac{v^2}{2g} - z_i\right) \times \rho g \tag{2.8}$$

In the current case the values obtained according to this method, for an imposed internal diameter of 2 inches:

- $\Delta P_{Total} = 0.94\ mbar < 1.5\ mbar$;
- $v = 2.34\ m/s < 10\ m/s$.

Since the results used in both methods are quite similar, it is considered that the sizing has been done correctly. Thus, it will be necessary to install a steel pipe with an internal diameter of 2 inches.

2.2. Burner Selection

The burner to be selected will be an integral and crucial part of this whole test stand, therefore, must meet several essential characteristics, namely: be able to model different power levels, allowing the simulation of different heat streams with variable power, typical in the industrial environment; and to produce a stable combustion and flame over time.

In a pre-mix burner, a fuel, and an oxidant (typically air) are thoroughly mixed before combustion begins. This type of burner usually offers shorter and more intense flames. In return this can cause high temperature regions in the flame, leading to non-uniform heating and higher NOx emissions.

In a diffusion burner the fuel and oxidant remain separate prior to combustion. Combustion begins when the oxidant/fuel mixture is within the flammability range. In cases where oxygen/fuel mixing occurs diffusion burners are more commonly used due to safety concerns. They usually have larger flames than pre-mix burners and have a more uniform temperature and heat flow.

Typically, in diffusive burners, control is difficult because it is necessary to manipulate the air flow and the flow of natural gas to maintain stable combustion, without large oscillations. However, monobloc burners with diffusive flame automatically adjust air flow, keeping a stable combustion. The adjustment of the power output is usually made using PID's which are responsible for controlling the flow of natural gas. The combination of the mechanical and electronic components reduces costs and makes this type of burner more economically viable than other solutions.

Diffusive flame burners can operate either in proportional control mode or in on/off mode.

For the design of the test stand, a diffusion type burner will be the most suitable as it allows to obtain a uniform adiabatic flame temperature and is much safer than pre-mixing burners.

It is intended a burner capable of producing several power ranges and a maximum power of approximately 200 kW. Consulting the catalogue of Riello S.p.A the selection made was of a Riello GULLIVER BS3/M (Figure 2.1) - Modulating burner, with its main characteristics to be presented in Table 2.1.

Table 2.1. Riello GULLIVER BS3/M – Main Features.

Heat Output [kW]	Weight [kg]	Net unit price [€]	Included accessories
48/79 - 195	16	3369.00	Gas Ramp; temperature modulation kit

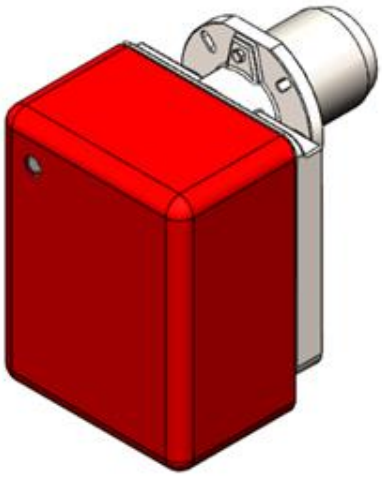

Figure 2.1. Riello BS3/M – 3D CAD.

2.3. Combustion and mixing/dilution chamber

Once the burner has been selected, the next step is the sizing and construction of the combustion and mixing/dilution chamber.

The purpose of the chamber is to confine the diffusive flame produced by the burner, while serving as a medium for mixing between the combustion products and a dilution air.

The mixture between combustion products (which are at adiabatic flame temperature) and a dilution air (assumed at 25°C) allows the outlet temperature to be modelled. This will be possible by controlling the flow of dilution air into the combustion chamber. The flow rate values, and their calculation method will be presented in Section 2.4.

As the design adopted (Figure 2.2), based on cases already existing in the industry, it was sought to design a combustion chamber with a cylindrical shape in which 4 crucial components are denoted: a refractory cement/brick cover to which the burner will be attached; a cylindrical piece formed in high alumina and temperature refractory concrete which aims to encapsulate the diffusive flame produced by the burner, preserving the remaining components from a direct contact at high temperatures; An intermediate steel cylinder which is responsible for directing the mixture of combustion products and dilution air towards a heat exchanger located downstream of the combustion chamber; and an outer, adiabatic casing, responsible for containing all the gases inside, preventing heat loss to the outside and also allowing the dilution air to be insufflated.

The first step in sizing is to obtain the dimensions of the cylindrical piece of refractory concrete. For this it is essential to know the typical dimensions of the diffusive flame

produced by the burner. Using the manufacturer's catalogue and for a maximum power of approximately 200 kW (Figure 2.3), the characteristic dimensions of the flame will be:

- $L_{min} \approx 500$ [mm] = 0.5 [m];
- $L_{max} \approx 800$ [mm] = 0.8 [m];
- $D_{min} \approx 400$ [mm] = 0.4 [m];
- $D_{max} \approx 500$ [mm] = 0.5 [m].

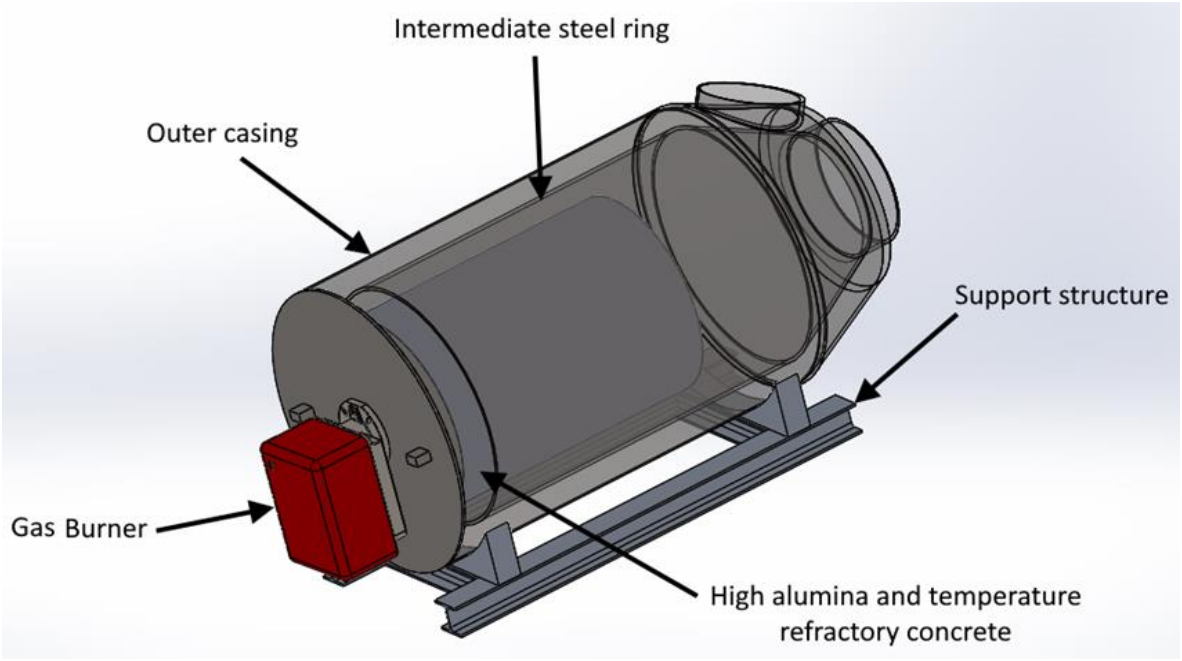

Figure 2.2. Isometric view of the combustion chamber.

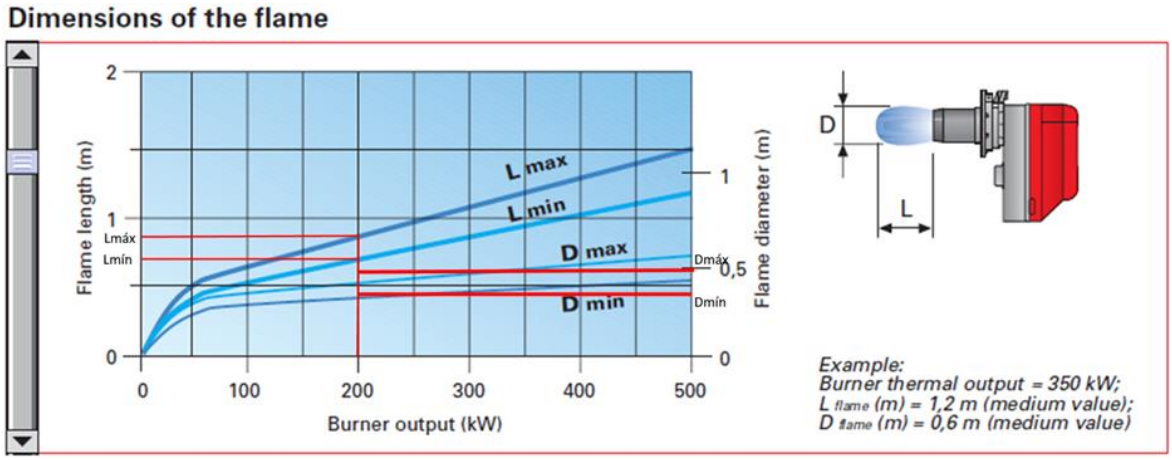

Figure 2.3. Diffusive flame dimensions.

The variations in length and diameter of flame are quite common in this type of burners due to an interaction between the flame emitted by the burner and the characteristics of the

environment and space where the flame is produced. Therefore, it is common for manufacturers to provide these dimensions within ranges, as in the present case.

There is, however, no mention in the manufacturer's catalogue of the minimum size of the flame encapsulation. Thus, and following a good practice commonly adopted for diffusive flame burners, the dimensions to be considered for encapsulation should be 20% greater than the maximum flame size limits, avoiding excessive wear of the material and making combustion safer.

The size of the high alumina, high temperature refractory concrete encapsulation shall be:

- L = 960 [mm] = 0.96 [m];
- D = 600 [mm] = 0.6 [m].

For the design of the intermediate steel cylinder, only the maximum velocity of the dilution air that circulates there and the associated pressure drop were taken into consideration. To avoid air velocity exceeding 15 m/s, a diameter of 740 mm was considered. The transition section of the gases from the combustion chamber to the downstream heat exchanger was kept as smooth as possible, avoiding abrupt variations which could induce pressure losses in the flow.

Similarly, the outer casing was sized to ensure that the pressure loss of the flow circulating between it and the intermediate ring is reduced. Thus, a diameter of about 900 mm was considered for the outer casing.

As previously stated, to avoid a sharp transition and to allow energy exchanges between the dilution air and the combustion products, a total length of this combustion chamber of approximately 1650 mm was chosen. There is also a ventilated air intake of approximately 310 mm to maintain a velocity below 20 m/s.

The diameters adopted are a function of the high flow rates required in some of the cases under analysis. These flows will be obtained in Section 2.4.

Finally, note the characteristic position of the dilution air insufflation, which is only intended to allow continuous cooling of the intermediate steel cylinder and subsequently of the refractory cylinder, following the trajectory represented in Figure 2.4.

During the development of this first combustion chamber design, several problems associated with it became evident, which in the end were crucial in the abandonment of this idea.

The associated problems identified were:

- Difficulty in obtaining a refractory cylinder with the required dimensions on the market;
- Difficulty in supporting a piece of refractory concrete with a considerable mass;
- Difficulty in supporting the intermediate steel ring;
- Difficulty in guaranteeing the centrality and concentricity of the pieces. The installation of centering rings would be possible, but due to the high temperatures and temperature variations there would be a constant expansion and contraction of the constituent steel, which would result in the occurrence of material fatigue;
- Similarly, the intermediate ring would be subject to constant expansion and contraction, which could lead to fatigue over time;
- Lack of guarantees of the ability of the dilution air to effectively cool all constituent parts;
- High economic investment in the in-house construction of this project.

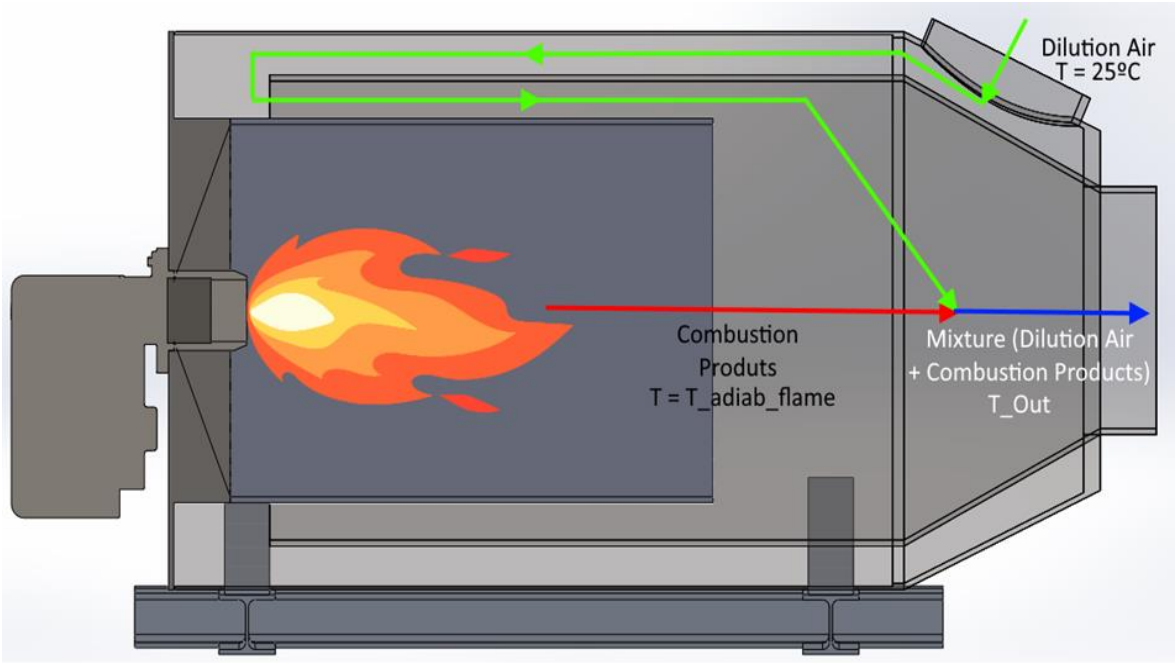

Figure 2.4. Cut of the combustion chamber and path of the insufflation air and combustion products.

After abandoning the original idea, contact was sought with companies in the field of producing ceramic industrial kilns. The adoption of a collaboration/acquisition with a

company specialist in this area allows problems associated with material fatigue to be avoided, thus absorbing the expertise they have in this area.

The solution found in collaboration with the nearby company "*Induzir - Indústria e Comércio de Equipamentos, Lda*" involves the creation of a combustion and mixing/dilution chamber with a flat-walled configuration, which also permits dilution air ventilation and the extraction of the mixture of gases + dilution air. Due to the company's experience with similar projects, the quality and functionality of the entire assembly can be guaranteed.

2.4. Dilution Air

As stated above, dilution air insufflation allows the temperature of the combustion products (which are at a temperature equal to the adiabatic flame temperature) to be lowered to an imposed test temperature.

The burner can operate with various levels of excess air, which consequently causes variations in adiabatic flame temperature. The dilution air flow rate must take this into account, as well as the power at which the burner operates. The easiest way to obtain, for a given power and excess air condition, the air flow rate to be supplied is through the development of an algorithm and its application in a script. The MATLAB software will be used to develop this algorithm.

In fact, two different scripts will be used. The first allows to obtain the net calorific value of the natural gas for a given composition (obtained from https://www.ign.ren.pt/) and the second allows, among other parameters, to obtain the flow rate of dilution air to be insufflated so that the mixture will be at a certain predefined temperature.

Note that in both scripts the gases will be treated as perfect gases.

The steps required to obtain the LHV of natural gas can be found in APPENDIX A.

In Figure 2.5 is presented a flowchart that allow to describe the first Script developed.

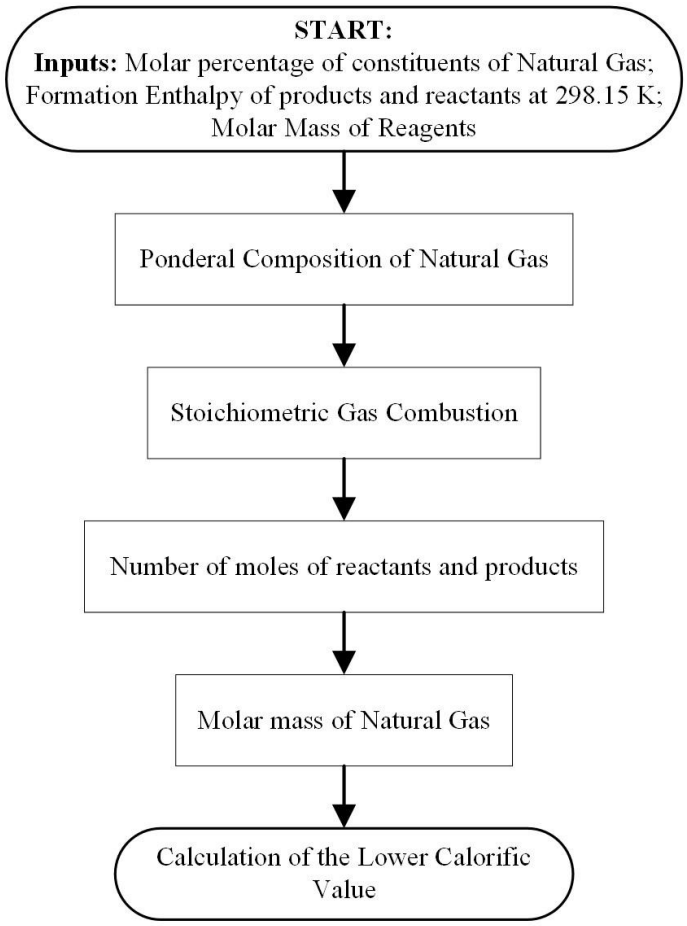

Figure 2.5. LHV calculation flowchart.

After running the algorithm developed for the calculation of the LHV it is possible to obtain, for the molar percentage of each constituent of Natural Gas considered in Table 2.2, the result: $LHV = 47.13177 \left[\frac{MJ}{kg}\right] = 857.427 \left[\frac{MJ}{kmol}\right]$.

Table 2.2. Molar percentage of each constituent of Natural Gas.

	CH4	C2H6	C3H8	C4H10i	C4H10n	C5H12i	C5H12n	C6H14n	N2	CO2
$N_{R.P}$	87.885%	8.056%	1.378%	0.108%	0.158%	0.022%	0.018%	0.02%	1.088%	1.266%

With the LHV calculation performed, it is possible to move on to the development of the second script. Here the objectives are to calculate the adiabatic flame temperature (temperature of the gases immediately after combustion has taken place and before any heat loss or exchange) for a given excess air set, calculate the flow rate of combustion products and finally calculate the flow rate of dilution air to be supplied so that the energy balance at the output meets the temperature conditions imposed.

The algorithm developed to perform these calculations (Figure 2.7) starts by obtaining the number of moles of natural gas for a given burner power. Thus, starting from the percentage by weight of each constituent, it is possible to obtain the number of moles and the composition by weight of the natural gas. The stoichiometric coefficients are then obtained for theoretical combustion and then for real combustion with imposed excess air.

Following the work developed by P. Carvalheira [26] and according to the first law of thermodynamics (Equation (2.9)):

$$Q_{R-P} - W_{R-P} = U_P - U_R \tag{2.9}$$

In the previous equation it is assumed that the work done by the system on the neighbourhood is positive, therefore in Equation (2.10):

$$W_{R-P} = \int_R^P p dV \tag{2.10}$$

For isobaric processes, the pressure is held constant, so Equation (2.10) can take the form of Equation (2.11):

$$W_{R-P} = p(V_P - V_R) \tag{2.11}$$

For adiabatic processes $Q_{R-P} = 0$ so Equation (2.9) can take the form of Equation (2.12):

$$-p(V_P - V_R) = U_P - U_R \tag{2.12}$$

Since for ideal gases enthalpy does not depend on pressure, Equation (2.12) takes the form:

$$H_P - H_R = 0 \Leftrightarrow H_P^\circ = H_R^\circ \tag{2.13}$$

With:

$$\begin{cases} H_R^\circ = \sum_{Reagents} n_i \Delta \tilde{h}_i^\circ \\ H_P^\circ = \sum_{Products} n_i \Delta \tilde{h}_i^\circ \end{cases} \tag{2.14}$$

Using Equation (2.13), for an adiabatic isobaric combustion, both sides of the equation have equal value. Thus, knowing the enthalpy of formation of the reactants (which enter at 25°C), it is possible using an iterative cycle to obtain the adiabatic flame temperature (temperature of the combustion products) which equals both sides.

Once the adiabatic flame temperature has been calculated, there are 1 of 2 solutions to choose from: either to obtain the flow rate to be blown to obtain a given outlet gas temperature, or to obtain the outlet gas temperature for a given air flow rate.

Using an energy balance for the mixture between combustion products and dilution air (Equation (2.14)) and imposing an output temperature, it is possible to obtain the value of the air flow to be insufflated.

$$\begin{aligned} n_{Air,Dilution} \times \left(H_{Air,Dilution@Toutlet} - H_{Air,Dilution@298,15}\right) \\ = a \times \left(H_{CO_2@Tflame} - H_{CO_2@Toutlet}\right) \\ + b \times \left(H_{H_2O@Tflame} - H_{H_2O@Toutlet}\right) \\ + c \times \left(H_{N_2@Tflame} - H_{N_2@Toutlet}\right) \\ + d \times \left(H_{O_2@Tflame} - H_{O_2@Toutlet}\right) \end{aligned} \quad (2.15)$$

To confirm the validation of the implemented algorithm, imposing an excess of air of 10% and a burner power of 150 kW the calculation of the supply flow values for different imposed outlet temperatures was made. This calculation is shown in Figure 2.6.

As expected, due to the high temperature of the combustion products, to obtain lower outlet temperatures, the air flow to be blown at 25 °C must be quite high, in this case in the order of 1 m/s. At higher outlet temperatures, the supply flow requirement decreases, as expected.

The calculations that serve as the basis for the development of this algorithm are in APPENDIX B.

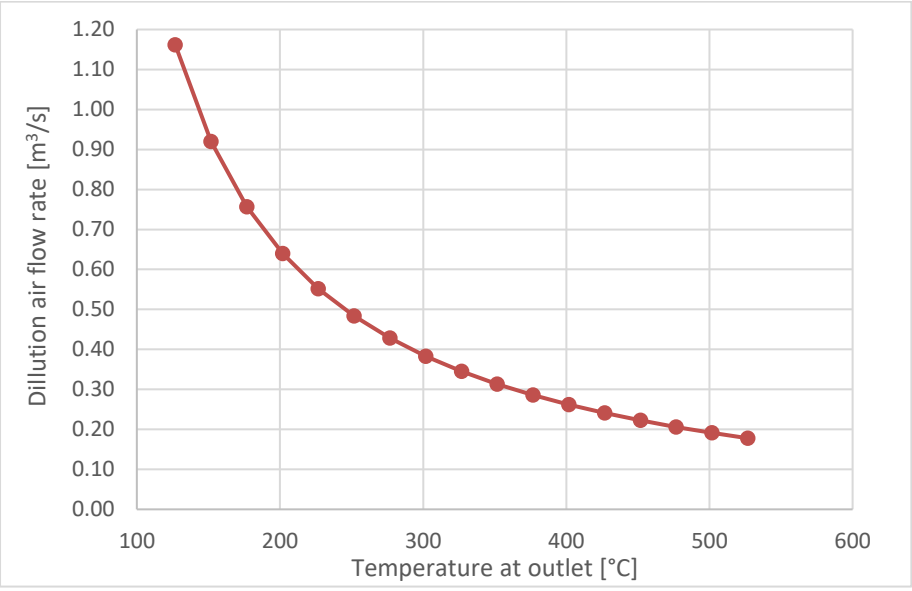

Figure 2.6. Dilution air flow rate variation with temperature for an excess air of 10% and a burner power output of 150 kW.

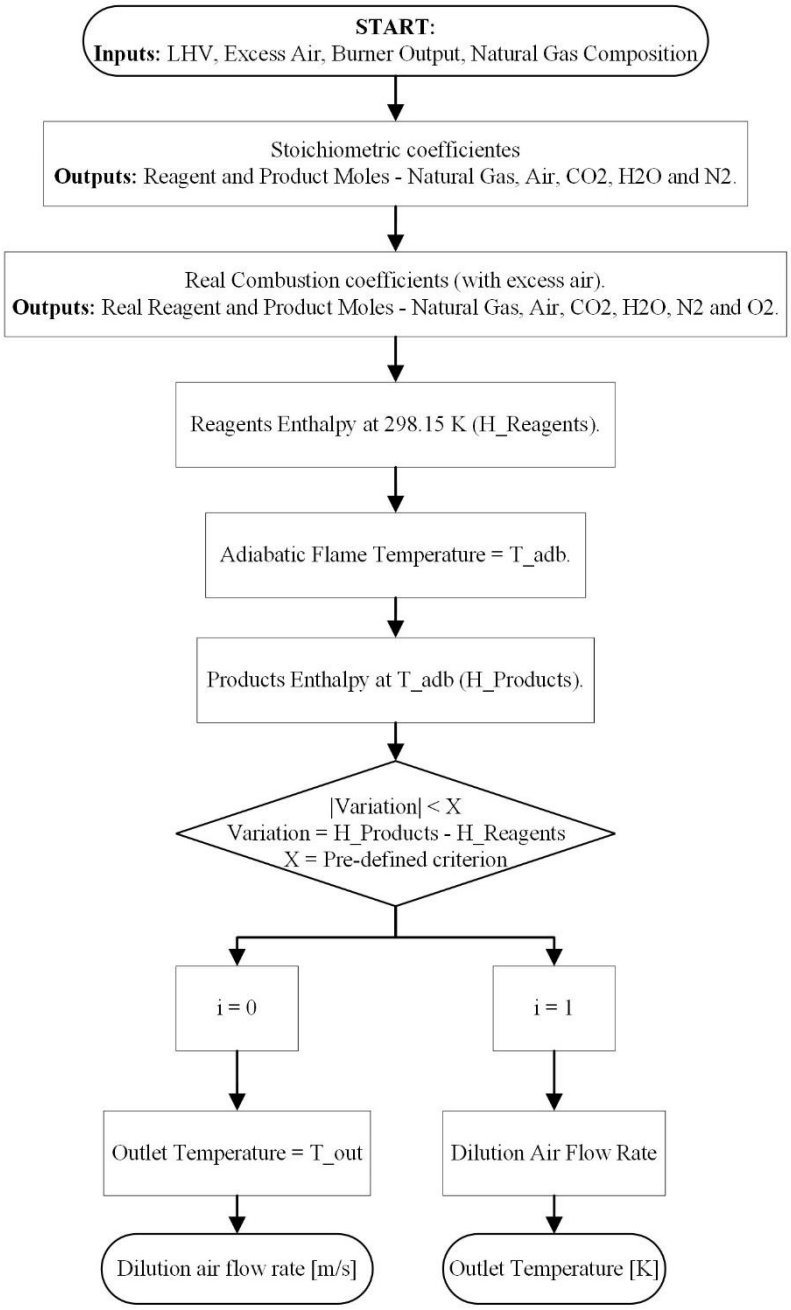

Figure 2.7. Flowchart for calculation of the dilution air flow rate.

2.5. Dimensioning a heat exchanger

At this stage of the development of the test rig it is necessary to dimension a compact heat exchanger, which allows the heat transfer between the mixture of combustion gases and dilution air leaving the combustion and mixing/dilution chamber and an intermediate thermal oil which will later serve as connection to the ORC based power cycle developed by SCIVEN, serving as its hot source.

The use of a compact heat exchanger is due to the restricted space where the whole test stand will be assembled, allowing to obtain a smaller heat exchanger than for example a shell-and-tube heat exchanger.

Due to the complexity of dimensioning this type of equipment and the number of iterations necessary to obtain the final values of each of the variables involved, a script was developed using MATLAB software.

The book developed by F. P. Incropera *et al.* [27], and the study developed by J. S. Pereira *et al.* [28] serve as a basis for the development of the MATLAB script, which allowed the construction of a support flowchart (ANNEX E) and a better knowledge of the heat transfer equations intrinsic to the design of a compact heat exchanger.

The first step in dimensioning the compact heat exchanger is to define the positioning of the piping that allows the heat exchange between the external gases and an internal thermal oil. For this case, the piping was finned on the outside and arranged in a parallel distribution like the one found in Figure 2.8, allowing a direct connection between passages/levels, thus avoiding piping with exaggerated diameters, which cause disproportionate dimensions to the heat exchanger. Placing the fins on the outside increases the contact area between the gases and the pipe, reducing thermal resistance and enhancing heat exchange.

Non-geometric inputs for the dimensioning of the heat exchanger include the temperature, pressure, and mass flow rate of the mixture of gases + dilution air leaving the combustion chamber, the mass fraction of each constituent of this mixture and the total thermal oil mass flow rate and it´s temperature at the inlet. As adjustable geometric inputs, the following are used: the length of the exchanger pipes, the width of the exchanger, the internal and external diameters of the piping, the number of passages/levels to be considered and the thickness, diameter, and pitch of the fins.

Several temperature values are also defined, that serve as an initial guess, which will be updated throughout the execution of the script. These temperatures are the outlet temperature of the gases from the heat exchanger and the outlet temperature of the thermal oil from the heat exchanger.

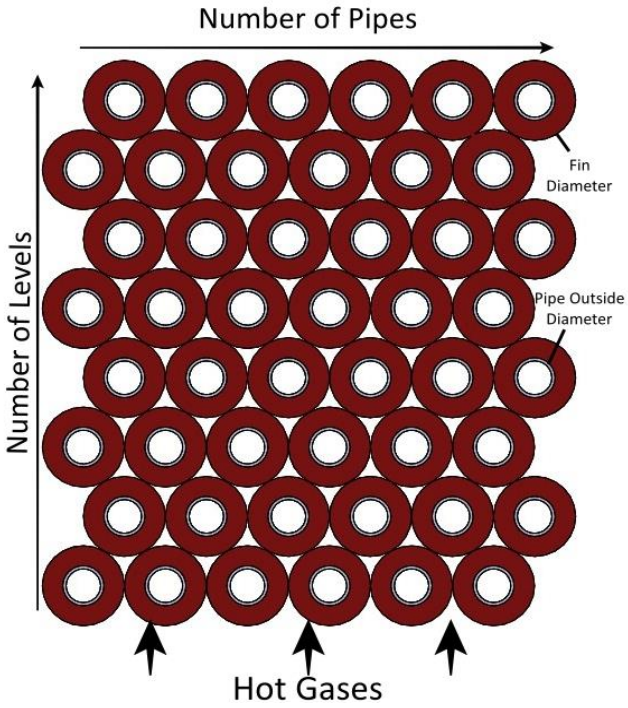

Figure 2.8. Adopted geometry for the piping of the compact heat exchanger.

To correctly dimension the heat exchanger, it is necessary to determine the overall heat transfer coefficient (U). To determine U it is necessary to know the values of the heat transfer coefficients on the thermal oil side (interior, h_f) and on the gas side (exterior, h_g), to know the conduction thermal resistance of the tube wall $\left(R_{t_{g,i}}\right)$ and the thermal resistances resulting from possible fouling $\left(R_{f,int}\ e\ R_{f,ext}\right)$.

Thus, a brief explanation of the calculation of each of these coefficients will be given, followed by an explanation of the iterative development in the MATLAB Script.

2.5.1. Overall Heat-Transfer Coefficient

2.5.1.1. External heat-transfer coefficient

Typically, convection and radiation mechanisms play an important role in the heat exchanges between hot gases and a thermal oil, so the gas-side heat transfer coefficient can be written in the form of Equation (2.16), with $h_{g,conv}$ corresponding to the gas-side convective heat-transfer coefficient and $h_{g,rad}$ corresponding to the gas-side radiative heat-transfer coefficient. However, in the present case, the radiative heat exchange coefficient will be ignored, since operating temperatures of the mixture that is intended to be used and simulate industrial conditions are relatively low and consequently so are the radiative

exchanges. Since radiative exchanges will be of a magnitude much smaller than convective exchanges, its disregard is justified to save computational resources.

$$h_g = h_{g,conv} + h_{g,rad} \tag{2.16}$$

According to J. S. Pereira *et al.* [28], the convective heat transfer coefficient can be obtained using Equation (2.17).

$$h_{g,conv} = St \times G_g \times c_{p,g} \tag{2.17}$$

With St corresponding to the Stanton number, obtained using Equation (2.18), G_g to the maximum mass velocity of the gases, calculated using Equation (2.19), and $c_{p,g}$ is the gases specific heat.

$$St = \frac{j_h}{Pr_g^{\,2/3}} \tag{2.18}$$

$$G_g = \frac{\dot{m}_g}{A_{ff}} \tag{2.19}$$

With, j_h corresponding to a factor obtained experimentally, the Colburn factor, which is a function of the geometry adopted and the Reynolds number (Re_g), which can be calculated using Equation (2.20). Pr_g corresponds to Prandtl's number.

With, $\dot{m}_g$ representing the mass flow rate of the mixture gases + dilution air and A_{ff} corresponding to the free flow area of the fin spacing (cross section perpendicular to the direction of flow).

$$Re_g = G_g \times \frac{D_h}{\mu_g} \tag{2.20}$$

With, D_h corresponding to the hydraulic diameter and given by Equation (2.21), and μ_g to the dynamic viscosity of the mixture gases + dilution air.

$$D_h = \frac{4A_{ff}}{P_{ff}} \tag{2.21}$$

With, P_{ff} corresponding to the free flow perimeter of the fin spacing.

2.5.1.2. Internal heat-transfer coefficient

For the calculation of the internal heat transmission coefficient, Equation (2.22) is followed [28].

$$h_{f,i} = Nu_{fl} \times \frac{k_{f,i}}{D_{t,int}} \tag{2.22}$$

With, Nu_{fl} corresponding to the Nusselt number and given by Equation (2.23) (Gnielinski correlation), $k_{f,i}$ corresponding to the thermal conductivity of the thermal oil and $D_{t,int}$ to the internal diameter of the pipe.

$$Nu_{fl} = \frac{(f_i/8) \times \left(Re_{f,i} - 1000\right) \times Pr_{f,i}}{1 + 12.7 \times (f_i/8)^{1/2} \times \left({Pr_{f,i}}^{2/3} - 1\right)} \tag{2.23}$$

Where $Re_{f,i}$ represents the Reynolds number and $Pr_{f,i}$ the Prandtl number of the thermal oil. f_i represents the friction factor and is given by Equation (2.24).

$$f_i = \left(0.79 \times ln\left(Re_{f,i}\right) - 1.64\right)^{-2} \tag{2.24}$$

The previous equations apply for the case of smooth pipes. If the application of corrugated pipes is to be evaluated, the calculation of Nu_{fl} will take the form of Equation (2.25).

$$Nu_{fl} = 0.3741\phi^{0.25}[Re_{f,i} - 1500]^{0.74}{Pr_{f,i}}^{0.44} \tag{2.25}$$

With ϕ corresponding to a dimensionless factor calculated using Equation (2.26) which is a function of the height (e) and pitch ($pitch$) of the helical tube [29].

$$\phi = \frac{e^2}{pitch \times D_{t,int}} \tag{2.26}$$

2.5.1.3. Calculation of the Overall Heat-Transfer Coefficient, U

U can be calculated using Equation (2.27), where $R_{f,int}$ and $R_{f,ext}$ correspond to the internal and external fouling factors, respectively, RA to the ratio between the internal and external heat transfer area, $R_{t_{g,i}}$ to the thermal resistance of the pipe wall (obtained using Equation (2.28)), $D_{t,ext}$ to the external diameter of the pipe and $k_{t,i}$ to its thermal conductivity.

It is also necessary to calculate the overall efficiency of the finned surface $\left(\eta_{f,sur}\right)$ so Equation (2.29) can be used.

$$U = \frac{1}{\frac{1}{h_{f,i} \times RA} + \frac{R_{f,int}}{RA} + R_{t_{g,i}} + R_{f,ext} + \frac{1}{h_g \times \eta_{f,sur}}} \tag{2.27}$$

$$R_{t_{g,i}} = \frac{D_{t,int} \times \ln\left(D_{t,ext}/D_{t,int}\right)}{2 \times k_{t,i} \times RA} \tag{2.28}$$

$$\eta_{f,sur} = 1 - \frac{A_{fin}}{A_{t,ext}} \times \left(1 - \eta_{fin}\right) \tag{2.29}$$

With, A_{fin} corresponding to the total finned area and η_{fin} to the efficiency of each individual fin.

2.5.2. Heat Transfer Calculation

The heat transferred, at a certain control volume, can be calculated using Equation (2.30), where U_i is calculated based on that described in the previous subchapters. F_{PH_i} corresponds to a correction factor, which in this case is assumed equal to 1, and $LMDT_i$ corresponds to the logarithmic mean temperature difference of a given control volume that can be calculated using Equation (2.31).

$$\dot{Q}_{f,i} = U_i \times A_{t,ext} \times F_{PH_i} \times LMDT \tag{2.30}$$

$$LMDT = \frac{\left(T_{g,in} - T_{f,out,i}\right) - \left(T_{g,out} - T_{f,in,i}\right)}{ln\left(\frac{T_{g,in} - T_{f,out,i}}{T_{g,out} - T_{f,in,i}}\right)} \tag{2.31}$$

With, $T_{f,in,i}$ and $T_{f,out,i}$ corresponding to the inlet and outlet temperatures, respectively, of the thermal oil at a certain control volume. $T_{g,in}$ and $T_{g,out}$ correspond to the inlet and outlet temperatures, respectively, of the mixture gases + dilution air.

2.5.3. Development of the MATLAB Script

Knowing the general equations involved in the design of a compact heat exchanger, the necessary conditions for the development of a script that allows the automation of this type of design are met.

The flowchart represented in ANNEX E, serves as a basis for the development of this script.

The Script starts with the introduction of the inputs mentioned at the beginning of this chapter, where the inputs characterising the mixture gases + dilution air are obtained from the Script developed in Section 2.4, the geometric inputs and the initial guesses for the temperature values are defined by the engineer.

Based on the inlet gas temperature and the initial guess of the outlet gas temperature it is possible, by imposing the inlet temperature of the thermal oil, to obtain a first approximation of the outlet oil temperature, using a global energy balance.

Once the first approximations (initialisation) have been defined, it is possible to start the development of the iterative cycles that characterise this dimensioning.

Although the iterative cycles that characterize this script are defined from "outside in" it makes sense to perform a brief explanation looking at the script from "inside out".

Since the thermal oil's properties change as it absorbs heat/increases temperature, it makes sense to update its properties along the pipe, by level. In order not to make the script execution time excessive it was previously defined the subdivision of the pipe into 10 sections with the same length. Since the thermal oil is in the liquid state and will never vaporize, this approach is considered sufficient to obtain reliable results.

Thus, the innermost cycle of this script starts by subdividing each tube into 10 sections. For the first section of the first pipe the inlet temperature of the thermal oil is equal to the inlet fluid temperature introduced. Through an iterative cycle, it is possible to obtain the fluid temperature at the outlet of that same section, calculating the heat absorbed by the thermal oil and updating that temperature until the heat released by the gases is equal to the heat absorbed by the thermal oil. To perform the calculation of the heat given off by the gases it is first necessary to obtain the value of the general heat transfer coefficient. To obtain the value of U it is necessary to obtain the internal heat transfer coefficient and the external heat transfer coefficient, calculated in an outermost cycle, between levels, which depends on the temperature of the mixture gases + dilution air in the section immediately before and in the section immediately after the location of the pipes.

When this condition is met, the temperature of the next section is updated, and the process is repeated through all 10 sections of the pipe.

The same process takes place at the pipe level, where it is again calculated whether the power absorbed by the thermal oil is equal to the power given off by the gases.

When the cycle for obtaining the thermal oil outlet temperature of each tube is complete, the power absorbed in the tube by the thermal oil can be calculated. Due to the defined geometric conditions, the power absorbed by each tube will be the same within the same level and the power absorbed by all the thermal oil in one level/passage can thus be obtained. However, in this case the power absorbed by the oil will not correspond to the

power given off by the gases, so it is necessary to update the temperature of the gases until the energy balance is satisfied.

When changing the gas temperatures, it is necessary to go back through the iterative cycles, going through the convergence conditions again updating all the calculated temperatures and power. When the total power given off by the gases equals the total power absorbed by the thermal oil, the script is completed, allowing the following outputs to be obtained: outlet temperature and thermal oil velocity, mixture gases + dilution air outlet temperature and power absorbed by the thermal oil, among other calculable geometric outputs.

2.5.4. Parametric Analysis

After the development of the MATLAB script it remains to evaluate its validity and different geometries and input parameters defined by the user. These tests allow to analyse the influence that different inputs may have on the total power absorbed by the thermal oil.

The first step is to develop a strategy to analyse the influence of some of these parameters.

Therefore, 3 different pipe sizes that are likely to be found on the market have been selected:

- Piping 1: $D_{ext,1} = 25.4\ mm;\ D_{int,1} = 21.4\ mm;$
- Piping 2: $D_{ext,2} = 38.1\ mm;\ D_{int,2} = 30.1\ mm;$
- Piping 3: $D_{ext,3} = 18\ mm;\ D_{int,3} = 15\ mm;$

Note that the height value is obtained using the number of levels defined as input and the fin diameter, which is twice the external diameter of the piping. The number of pipes per level is obtained by imposing a total width on the exchanger.

To assess the influence that the width of the heat exchanger, and consequently the number of tubes per level, will have on the absorbed power, for each one of the tubes dimensions, two different values of the exchanger width were evaluated.

In summary, 6 different geometries were used for each set of results to reliably assess the variation in outputs obtained. In Table 2.3 is presented a summary of the geometries used for the analysis. Note that the thermal oil flow rate imposed for each of the geometries is the one that allows to obtain an oil velocity inside the pipes slightly below 3 m/s, this being the

maximum recommended velocity. Higher velocities allow an increase in the turbulence of the flow and consequently an increase in the internal heat-transfer coefficient but have the undesired effect of creating greater friction and a pressure drop greater than the admissible which will punish the circuit pump [30]. A speed of 3 m/s is the best compromise between these two criteria.

An initial, basic series was conducted to serve as a starting point for the evaluation. In the second series of tests the effect of varying the oil inlet temperature was evaluated, increasing the oil temperature from 80°C (in the first series) to 100°C. In the third series the variation of the distance between fins and consequently the number of fins per pipe was evaluated. In the fourth series, the influence of the number of levels (increasing from 5 to 7) was evaluated, for the oil temperature imposed in the second series (100°C). In the fifth series, the influence of changing the material of the tubes and fins was determined, assuming copper in both cases (in all other series it was assumed that the tube would be composed of a typical steel and the fins of aluminium). In the sixth series the influence of using corrugated pipes in the construction of the heat exchanger was assessed.

Table 2.3. Geometric inputs used in parametric analysis.

Geometry	$D_{pipe,ext}$ [mm]	$D_{pipe,int}$ [mm]	Tube Length [m]	Exchanger Width [m]	$m_{f,total}$ [kg/s]
1	25.4	21.4	0.7	1	19
2	25.4	21.4	0.7	0.8	15
3	38.1	30.1	0.7	0.8	18.5
4	38.1	30.1	0.7	0.6	12.5
5	18	15	0.7	1	13.5
6	18	15	0.7	0.8	11

The results obtained for each of the series and geometries can be seen in Table 2.4.

Table 2.4. Parametric analysis of the power absorbed by thermal oil for 6 different geometries [kW].

	Geometry 1	Geometry 2	Geometry 3	Geometry 4	Geometry 5	Geometry 6
Serie 1	101.30	91.85	87.41	68.85	99.89	93.08
Serie 2	83.87	76.81	73.65	58.87	82.66	77.64
Serie 3	108.61	100.71	94.37	76.11	Diverge	102.87
Serie 4	Diverge	86.88	84.39	70.99	Diverge	Diverge
Serie 5	103.96	94.92	93.13	74.70	101.85	95.30
Serie 6	Diverge	102.24	100.64	82.61	Diverge	102.36

As expected, when the inlet temperature of the imposed oil increases, the power absorbed by it decreases (series 2). This is due to the lower temperature difference between the flow of gases and thermal oil, decreasing the mean logarithmic difference and consequently the absorbed power. The evolution is similar for all analysed geometries.

Compared to series 1, the values obtained for series 3 are higher for all geometries, which is to be expected since the number of fins per tube and consequently the external surface area of heat exchange is doubled.

Comparing series 4 with series 2 (series with equal fluid inlet temperature) by increasing the number of pipe levels the power absorbed increases. This is due to the considerable increase of the available heat transfer area. For series 4 the number of levels considered was 7 while for the other series it was 5.

Due to the higher thermal conductivity of copper, and consequently lower thermal resistance, the value of the overall heat-transfer coefficient will increase, increasing the power absorbed. Thus, comparing series 5 with series 1, where only the material of the pipes and fins is changed and the geometric characteristics were maintained, the power absorbed increases.

Finally, in series 6, the power absorbed will increase considerably when compared to series 1. This is expected due to the design of the corrugated pipes. These are responsible for inducing increased turbulence in the thermal oil flow and consequently increasing the internal and overall heat-transfer coefficients.

It should be noted that due to the intrinsic formulation of the MATLAB Script for several cases the convergence of the program is not possible. This is due to the low difference between the outlet gas temperature and the thermal oil temperature, resulting in reduced logarithmic mean differences.

Besides the previously described analysis, the influence of the evolution of some geometrical characteristics on the absorbed power was also evaluated.

The analysis was conducted for four different cases. In the first case (Figure 2.9), the influence of increasing the number of fins on the absorbed power was evaluated. Note that all other geometrical conditions and inputs remained constant. As expected, an asymptotic evolution occurs, with the effect of the increase in the number of fins on the absorbed power reducing as the number of fins increases. Thus, there is a limiting trend in the absorbed power.

In the second analysis only the total width of the heat exchanger and consequently the number of tubes per level was varied. As in the previous analysis, an asymptotic evolution is clearly observed (Figure 2.10), showing that as the exchanger width increases the increase in the absorbed power tends to decrease, converging, at the limit.

For the third analysis only the number of levels (and consequently the height) of the exchanger was varied. As in the previous analyses, it is observable that an asymptotic evolution occurs (Figure 2.11).

For the fourth analysis, the total mass flow rate of thermal oil circulating in the pipes was varied (Figure 2.12). Analogously to the previous analyses there is an asymptotic evolution for this case. As the fluid flow rate increases, the thermal oil velocity will also increase, resulting in an increase in the Reynolds number and consequently in the increase of the internal heat transfer coefficient. However, for very high flow rates (and consequently velocities) the influence of the Reynolds number increase on the absorbed power will tend to decrease.

Besides the geometrical evidences previously described, several other conclusions can be drawn from the analyses performed. The most important conclusion drawn is that the internal heat transfer coefficient is determinant in the value of the overall heat transfer coefficient and in the power absorbed by the thermal oil, relegating the influence of the external coefficient to second place. Due to the characteristics resulting from the calculation of the internal coefficient (see Section 2.5.1.2), which strongly depends on the Nusselt number, which in turn is a function of the Reynolds number and consequently of the flow velocity, for small velocities low values of absorbed power are verified, increasing with the increase of the flow velocity. Note that due to the geometric choice (piping layout and size) to obtain velocity values close to 3 m/s it was necessary to impose quite high total thermal oil flow rates, which will translate into small variations in thermal oil inlet and outlet temperatures when compared to the variation in gas flow inlet and outlet temperatures. This problem is, however, solved by decreasing the diameter of the pipes and the number of pipes per level, which allows the total flow rate of thermal oil in the exchanger to be reduced to obtain the same velocity values ($\approx$ 3 m/s). This associated with the increase in the number of levels/passages in the exchanger allows similar values of absorbed power to be obtained in relation to the cases previously described, observing, however, a temperature evolution of the thermal oil like that of the gas flow.

It would therefore be necessary to conduct a detailed economic analysis to assess which configuration would be advantageous: configuration with a smaller number of pipes but a higher total flow of thermal oil or configuration with a larger number of pipes but a lower total flow of thermal oil.

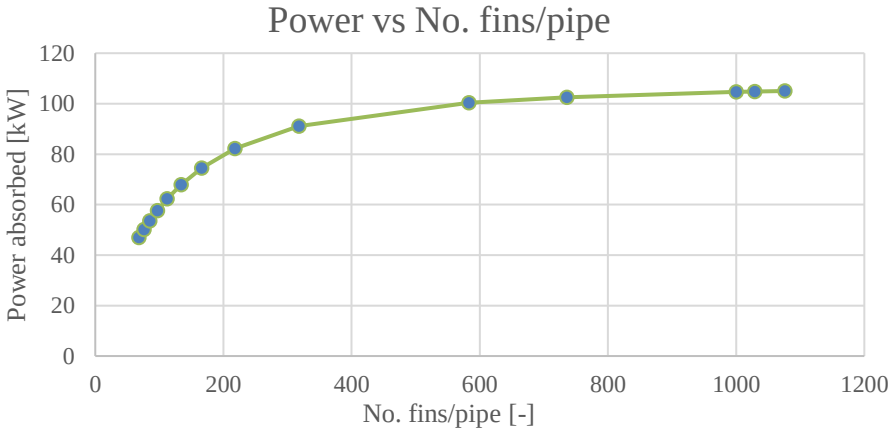

Figure 2.9. Evaluation of the increase in the number of fins per pipe on the absorbed power.

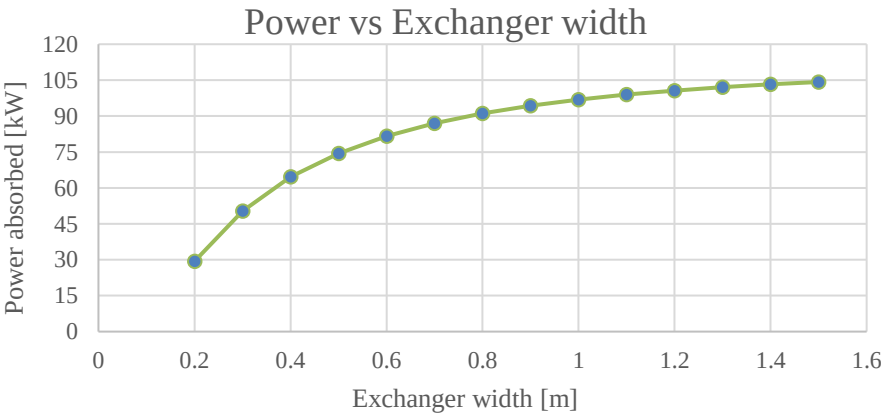

Figure 2.10. Evaluation of the increase of the exchanger width on the absorbed power.

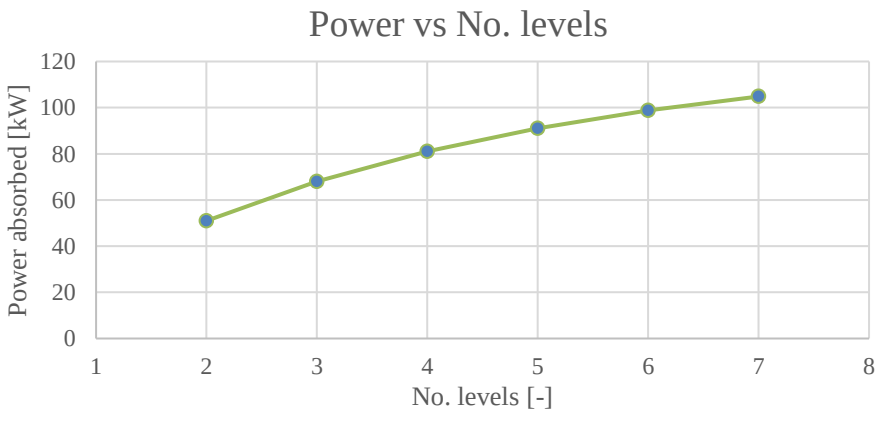

Figure 2.11. Evaluation of the increase in the number of levels in the absorbed power.

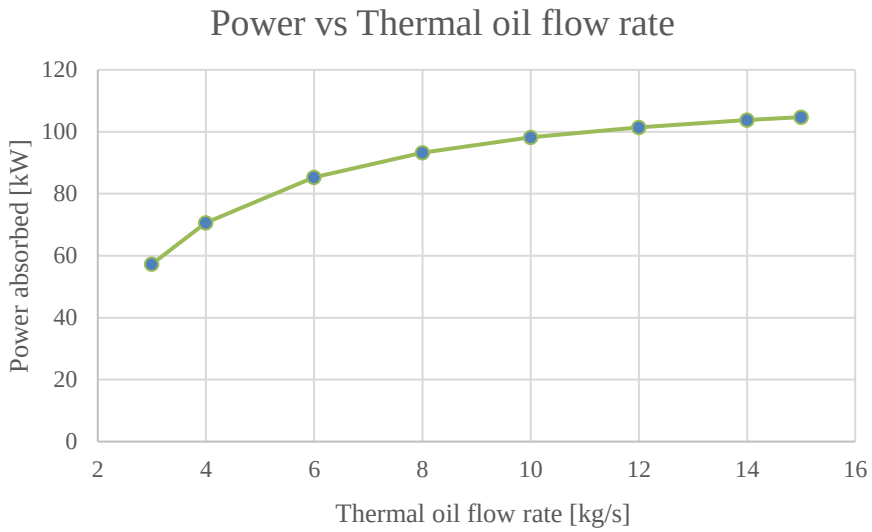

Figure 2.12. Evaluation of the increase of thermal oil flow rate on the absorbed power.

2.6. 3D drawing of the heat exchanger and the overall test stand

A general representation for the heat exchanger considered can be seen in ANNEX F. As previously stated, to decide which configuration to use, it will be necessary to conduct a detailed economic analysis.

In the ANNEX G it is possible to see the general configuration of the combustion and mixing/dilution chamber + centrifugal fan + heat exchanger + connecting ducts. Note that this new configuration was already developed having in mind the proposal presented by the company "*Induzir - Indústria e Comércio de Equipamentos, Lda*" being the dimensions remarkably close to the foreseen ones. In Table 2.5 there are foreseen dimensions for the combustion/mixing chamber and for the total set.

Table 2.5. Combustion and mixing chamber & overall test stand dimensions.

	Height [mm]	Width [mm]	Depth [mm]
Combustion and mixing chamber	1675	1000	1600
Overall test stand	1675	1825	4290

3. CONCLUSIONS

3.1. Overall conclusions

Globally it was possible to achieve the pre-defined objectives for this dissertation, where it began by defining waste heat, its potential, the typical temperatures of heat streams found in industry and the most used heat recovery systems. A comparison between 5 different studies evaluating the waste heat potential in the EU and/or in Europe was also conducted. Finally, an essential part of the test bench was developed, starting with the sizing of the natural gas supply network to the laboratory, the selection of a burner, the sizing of its combustion and mixing/dilution chamber and finally the development of a compact heat exchanger sizing model.

As stated in the introductory note the next decades will be challenging in terms of meeting environmental targets, so work should be done to achieve the goals that each country has set out to achieve. As noted in Section 1.4, the potential that waste heat presents in the EU/Europe is tremendous, so a focus on developing new technologies or improving existing heat recovery technologies should be an integral part of the strategy set to meet the objectives agreed, whether through the recycling of heat or its use for power generation.

The dimensioning of the compact heat exchanger proved to be quite challenging, however this objective was fulfilled within the previously defined criteria. From the development of the model in MATLAB and its parametric characterisation it was possible to obtain several conclusions:

- The influence of the internal heat-transfer coefficient on the calculation of the overall heat-transfer coefficient and consequently on the power absorbed by the thermal oil is far greater than the other variables involved in the calculation;
- Increasing the overall size of the exchanger almost always results in an asymptotic evolution of the power absorbed;
- The geometrical arrangement of the exchanger's pipework is not the one that allows the greatest compromise between its overall dimensions and the power absorbed;

- Increasing the external heat-transfer area, either by increasing the number of fins per tube or by increasing the number of tubes, allows the power absorbed by the thermal oil to be increased to a certain limit;
- The greater the difference between the inlet temperature of the thermal oil and the inlet temperature of the gas flow the greater the power absorbed;
- The use of materials with a higher thermal conductivity, such as copper, allows the absorbed power to be increased.
- For a combustion power of 195 kW the geometries analysed only allow a maximum of 110 kW of power to be absorbed.

With this work it was possible to verify that each case in the industry will have unique conditions with different design variables and therefore it will be necessary to analyse independently each one of them.

3.2. Future work prospects

Following the development of this work, the obvious steps to follow in the future would be:

- Detailed economic analysis of which geometrical configuration to follow for the heat exchanger;
- Construction and real experimental validation of the dimensioned heat exchanger;
- To obtain experimentally the Colburn factor (j_h) for the developed geometry and its analysis for other geometries. Throughout the development of the model it proved impossible to obtain the value of this factor for the developed configuration, so an approximation was used;
- To evaluate the influence that the use of different thermal oils will have on the absorbed power;
- Continuation and development of the test bench (dimensioning welded joints, bolted connections, among others);
- Connection of the assembly developed in this work to the ORC module and its experimental testing;

- Development of similar sizing models for different compact heat exchanger configurations.

BIBLIOGRAPHY

[1] Direção Geral de Energia e Geologia, Agência Portuguesa do Ambiente, ADENE, and LNEG, "PLANO NACIONAL ENERGIA E CLIMA 2021-2030 (PNEC 2030)," 2019.

[2] "ENERGIA E CLIMA EMISSÕES DE GASES COM EFEITO DE ESTUFA," Nov. 2021.

[3] Agência portuguesa do ambiente, "ROTEIRO PARA A NEUTRALIDADE CARBÓNICA 2050 (RNC2050)," 2019.

[4] Eurostat, "Final energy consumption by sector, EU-27." https://ec.europa.eu/eurostat/statistics-explained/index.php?title=File:Final_energy_consumption_by_sector,_EU-27,_2018_(%25_of_total,_based_on_tonnes_of_oil_equivalent).png#file (accessed Mar. 08, 2022).

[5] E. Woolley, Y. Luo, and A. Simeone, "Industrial waste heat recovery: A systematic approach," *Sustainable Energy Technologies and Assessments*, vol. 29, pp. 50–59, Oct. 2018, doi: 10.1016/J.SETA.2018.07.001.

[6] S. Brückner, S. Liu, L. Miró, M. Radspieler, L. F. Cabeza, and E. Lävemann, "Industrial waste heat recovery technologies: An economic analysis of heat transformation technologies," *Applied Energy*, vol. 151, pp. 157–167, Aug. 2015, doi: 10.1016/J.APENERGY.2015.01.147.

[7] H. Jouhara, N. Khordehgah, S. Almahmoud, B. Delpech, A. Chauhan, and S. A. Tassou, "Waste heat recovery technologies and applications," *Thermal Science and Engineering Progress*, vol. 6, pp. 268–289, Jun. 2018, doi: 10.1016/j.tsep.2018.04.017.

[8] S. Brueckner, L. Miró, L. F. Cabeza, M. Pehnt, and E. Laevemann, "Methods to estimate the industrial waste heat potential of regions - A categorization and literature review," *Renewable and Sustainable Energy Reviews*, vol. 38, pp. 164–171, 2014, doi: 10.1016/j.rser.2014.04.078.

[9] G. P. Panayiotou *et al.*, "Preliminary assessment of waste heat potential in major European industries," in *Energy Procedia*, 2017, vol. 123, pp. 335–345. doi: 10.1016/j.egypro.2017.07.263.

[10] M. Benedetti, D. Dadi, L. Giordano, V. Introna, P. E. Lapenna, and A. Santolamazza, "Design of a database of case studies and technologies to increase the diffusion of low-temperature waste heat recovery in the industrial sector," *Sustainability (Switzerland)*, vol. 13, no. 9, May 2021, doi: 10.3390/su13095223.

[11] Z. Su *et al.*, "Opportunities and strategies for multigrade waste heat utilization in various industries: A recent review," *Energy Conversion and Management*, vol. 229. Elsevier Ltd, Feb. 01, 2021. doi: 10.1016/j.enconman.2020.113769.

[12] A. Alexandre Amorim Coimbra Vale, D. João Ribau, and P. Armando Oliveira, "Estudo da Recuperação de Calor Residual e sua Aplicação à Indústria Cerâmica," 2018.

[13] R. Loni, G. Najafi, E. Bellos, F. Rajaee, Z. Said, and M. Mazlan, "A review of industrial waste heat recovery system for power generation with Organic Rankine

Cycle: Recent challenges and future outlook," *Journal of Cleaner Production*, vol. 287, Mar. 2021, doi: 10.1016/j.jclepro.2020.125070.
[14] M. Papapetrou, G. Kosmadakis, A. Cipollina, U. la Commare, and G. Micale, "Industrial waste heat: Estimation of the technically available resource in the EU per industrial sector, temperature level and country," *Applied Thermal Engineering*, vol. 138, pp. 207–216, Jun. 2018, doi: 10.1016/j.applthermaleng.2018.04.043.
[15] G. Bianchi *et al.*, "Estimating the waste heat recovery in the European Union Industry," *Energy, Ecology and Environment*, vol. 4, no. 5, pp. 211–221, Oct. 2019, doi: 10.1007/s40974-019-00132-7.
[16] C. Forman, I. K. Muritala, R. Pardemann, and B. Meyer, "Estimating the global waste heat potential," *Renewable and Sustainable Energy Reviews*, vol. 57, pp. 1568–1579, May 2016, doi: 10.1016/j.rser.2015.12.192.
[17] G. P. Hammond and J. B. Norman, "Heat recovery opportunities in UK industry," *Applied Energy*, vol. 116, pp. 387–397, Mar. 2014, doi: 10.1016/J.APENERGY.2013.11.008.
[18] U. Persson, B. Möller, and S. Werner, "Heat Roadmap Europe: Identifying strategic heat synergy regions," *Energy Policy*, vol. 74, no. C, pp. 663–681, 2014, doi: 10.1016/j.enpol.2014.07.015.
[19] J. M. Cullen and J. M. Allwood, "Theoretical efficiency limits for energy conversion devices," *Energy*, vol. 35, no. 5, pp. 2059–2069, 2010, doi: 10.1016/j.energy.2010.01.024.
[20] N. Nakićenović, P. V. Gilli, and R. Kurz, "Regional and global exergy and energy efficiencies," *Energy*, vol. 21, no. 3, pp. 223–237, Mar. 1996, doi: 10.1016/0360-5442(96)00001-1.
[21] X. Jeroen de Beer, M. Zabeti, and F. Stern, "Industrial Waste Heat Recovery Using ORC - Techno Economic Assessment," *Ecofys on Assignment by Siemens Energy*, 2017.
[22] M. Astolfi *et al.*, "Thermal Energy Harvesting - the Path to Tapping into a Large CO2-free European Power Source," 2022. [Online]. Available: www.kcorc.org/en/committees/thermal-energy-harvesting-advocacy-group/
[23] P. Marques and A. M. de M. Grade, "Projecto de Rede de Distribuição de Gás Natural," ISEC, Coimbra, 2014.
[24] "APTA." https://www.apta.pt/conteudos.php?idConteudo=208 (accessed Apr. 19, 2022).
[25] P. Renouard, "Nouvelle méthode pour le calcul des réseaux maillés de conduites de gaz," 1952.
[26] P. Carvalheira, "Problema de Cálculo da Temperatura de Chama Isobárica Adiabática," Coimbra, Mar. 2020.
[27] F. P. Incropera, D. P. Dewitt, T. L. Bergman, and A. S. Lavine, *Fundamentals of Heat and Mass Transfer*, vol. Sixth Edition. 2007.
[28] J. S. Pereira, J. Almeida, J. C. André, R. Mendes, and J. B. Ribeiro, "Modelling and experimental validation of the heat-transfer processes of a direct vaporization micro-scale ORC-evaporator for thermal degradation risk assessment," *Energy Conversion and Management*, vol. 238, Jun. 2021, doi: 10.1016/j.enconman.2021.114130.
[29] G. G. Cruz, M. A. A. Mendes, J. M. C. Pereira, H. Santos, A. Nikulin, and A. S. Moita, "Experimental and numerical characterization of single-phase pressure drop and heat transfer enhancement in helical corrugated tubes," *International Journal of*

Heat and Mass Transfer, vol. 179, Nov. 2021, doi: 10.1016/j.ijheatmasstransfer.2021.121632.

[30] L. A. Oliveira and A. G. Lopes, *Mecânica dos fluidos*. Lisboa: Lidel, 2020.

[31] H. Satyavada and S. Baldi, "Monitoring energy efficiency of condensing boilers via hybrid first-principle modelling and estimation," *Energy*, vol. 142, pp. 121–129, Jan. 2018, doi: 10.1016/j.energy.2017.09.124.

[32] S. Quoilin, M. van den Broek, S. Declaye, P. Dewallef, and V. Lemort, "Techno-economic survey of organic rankine cycle (ORC) systems," *Renewable and Sustainable Energy Reviews*, vol. 22, pp. 168–186, 2013, doi: 10.1016/j.rser.2013.01.028.

[33] A. Elsayed, M. Embaye, R. Al-Dadah, S. Mahmoud, and A. Rezk, "Thermodynamic performance of kalina cycle system 11 (KCS11): Feasibility of using alternative zeotropic mixtures," *International Journal of Low-Carbon Technologies*, vol. 8, no. SUPPL1, Jul. 2013, doi: 10.1093/ijlct/ctt020.

[34] K. Hu, J. Zhu, W. Zhang, and X. Lu, "A case study of an ORC geothermal power demonstration system under partial load conditions in Huabei Oilfield, China," in *Energy Procedia*, 2017, vol. 142, pp. 1327–1332. doi: 10.1016/j.egypro.2017.12.515.

[35] H. A. Al-Rawashdeh, M. R. Gomaa, R. J. Mustafa, and A. O. Hasan, "Efficiency and exergy enhancement of ORC powered by recovering flue gases-heat system in cement industrials: A case study," *International Review of Mechanical Engineering*, vol. 13, no. 3, pp. 185–197, 2019, doi: 10.15866/ireme.v13i3.16713.

[36] P. H. Barros Zarante, M. C. Vanegas Chamorro, and J. D. N. Polo, "Feasibility evaluation of the use Organic Rankine Cycle (ORC) technology for energy production from exhaust gases recovery: a case study of local industry in Colombia," *Contemporary Engineering Sciences*, vol. 11, no. 44, pp. 2173–2180, 2018, doi: 10.12988/ces.2018.85223.

[37] A. M. Pantaleo, J. Fordham, O. A. Oyewunmi, and C. N. Markides, "Intermittent waste heat recovery via ORC in coffee torrefaction," in *Energy Procedia*, 2017, vol. 142, pp. 1714–1720. doi: 10.1016/j.egypro.2017.12.554.

[38] V. R. Seifert, Y. M. Barbosa, J. A. M. da Silva, and E. A. Torres, "Rankine cycle power augmentation: a comparative case study on the introduction of ORC or absorption chiller," *Journal of the Brazilian Society of Mechanical Sciences and Engineering*, vol. 39, no. 11, pp. 4837–4848, Nov. 2017, doi: 10.1007/s40430-017-0903-9.

[39] L. Rocha-Meneses, J. C. Silva, S. Cota, and T. Kikas, "Thermodynamic, Environmental and Economic Simulation of an Organic Rankine Cycle (ORC) for Waste Heat Recovery: Terceira Island Case Study," *Environmental and Climate Technologies*, vol. 23, no. 2, pp. 347–365, Nov. 2019, doi: 10.2478/rtuect-2019-0073.

[40] H. Hjartarson, "Waste Heat Utilization at Elkem Ferrosilicon Plant in Iceland," 2009, [Online]. Available: www.hi.is

[41] G. Angelino, P. Ferrari, M. Gaia, G. Giglioli, and E. Macchi, "Heat recovery by organic Rankine cycle in ceramics firing ovens. Final report," 1982, doi: https://doi.org/.

[42] F. Schorcht, I. Kourti, B. M. Scalet, S. Roudier, and L. D. Sancho, "Best Available Techniques (BAT) Reference Document for the Production of Cement, Lime and Magnesium Oxide," pp. 419–421, 2013.

[43] G. David, F. Michel, and L. Sanchez, “Waste heat recovery projects using Organic Rankine Cycle technology-Examples of biogas engines and steel mills applications,” 2011.
[44] Z. Guzović, P. Rašković, and Z. Blatarić, “The comparision of a basic and a dual-pressure ORC (Organic Rankine Cycle): Geothermal Power Plant Velika Ciglena case study,” *Energy*, vol. 76, pp. 175–186, Nov. 2014, doi: 10.1016/j.energy.2014.06.005.
[45] R. F. Costa and F. J. N. da Silva, “Produção de energia elétrica a partir do aproveitamento do calor residual proveniente dos fornos de fusão do vidro,” 2019.
[46] A. C. Thekdi, “Industrial Waste Heat Recovery: Potential Applications, Available Technologies and Crosscutting R&D Opportunities,” 2014. [Online]. Available: http://www.osti.gov/scitech/

ANNEX A

Table A.1. Characteristics of the most common heat recovery processes in Industry - Adapted from [12]

Waste Heat Recovery Technology		**Efficiency [%]**	**Operating Status**	**Price Range [€/kW Recovered Heat]**	**Examples of application**
Heat Pump	Mechanical Compression	Up to 600	35 to 125°C	80 to 730	*Drying, Washing, Distillation, Evaporation, Space Cooling and DHW Heating Processes*
	Thermal Compression	150	100 to 200°C		
	RMV	1000 to 3000	----		
	RTV	----	7 to 14 bar		
Economiser		72 to 99 [31]	----	----	*Boiler feed water preheating*
Organic Rankine Cycle		10 to 20 [32]	80 to 300°C	1500 to 3500	*Industrial processes - metalworking and glass - and power generation plants*
Kalina Cycle		20 to 40% more efficient then ORC [33]	100 to 400°C	1100 to 1500	*Industrial processes - cement - geothermal power stations and thermal solar system*
Burner	Recuperative	40 to 60	250 to 870°C	----	*Burners without recovery or regeneration*
	Regenerative	60 to 85	> 700°C		
Thermal Wheel		50 to 85	-55 to 800°C	100 to 350	*Heat recovery in AHU's*
Heat Pipe		60 to 80	-70 to 540°C	----	*Heat recovery in AHU's, furnaces, and dryers*

ANNEX B

Table B.1. Comparison of Real and Theoretical Case Studies of ORC's

Industry [1]	Temperature [°C]	Thermal Power	Electrical Power	Efficiency [%]	Cost [€]	Cost - Real [€/kW]	Cost - Forecast [€/kW]	Used organic fluid	Evaporating Pressure [MPa]	Condensation Pressure [MPa]
Petrochemical - Abandoned Oil Well [34]	110	----	500 kW	8	----	----	----	R245fa	0.819	0.187
Cement - Exhaust Gases [35]	290	----	323.33 kW	15.9 - 16.7	860 105	----	2660	R245fa	2.5	----
Exhaust gases from an internal combustion engine [36]	504	----	188 kW	10.74	597 567	----	3179	R245fa	----	----
Food - Coffee Roasting [37]	120	288 kW	----	9.21	120 000	----	417	R227ea	----	----
Thermoelectric Power Plants [38]	175.6	----	409.53 kW	15.25	----	----	----	n-butane	3.796	----

[1] Green - Real Cases; Blue - Theoretical Cases.

Urban Waste - Terceira Island [39]	145-155	----	485 kW	25	----	----	----	R245fa	3.75	0.09
Chemicals and Plastics - Furnace Exhaust Gases [40]	220 - 450	----	9 200 kW	----	----	1335.0	----	Methylbenzene	----	----
Ceramics - Kiln exhaust gases [41]	220	----	350 kW	11.5	----	----	----	Tetrachloroethylene	----	----
Cement - Exhaust air from clinker cooler [42]	300 - 350	----	1 000 kW	----	4000000	4000	----	Pentane	----	----
Steelmaking - Exhaust gases [43]	150	----	200 kWe	10	1080000	4000	----	R245fa	----	----
Biogas Engines - Exhaust Gas [43]	180 - 470	----	145 kWe	20	540000	----	3724	Methylbenzene	----	----
Geothermal Field [44]	175	----	5 270 kW	14.1	----	----	----	Pentane	2	----
Glass - Exhaust gases from the melting process [45]	400	----	421.5 kW	16.9	1563370	----	----	HFO1336mzz(Z)	2.458	0.1

ANNEX C

Table C.1. Comparison between studies

Category	Study 1 (Industry Evaluation - EU)	Study 2 (Industry Evaluation - EU)	Study 3 (Evaluation of all sectors - global)	Study 4 (Industry Evaluation - EU)	Study 5 (Industry Evaluation - Europe)
Theoretical Potential	----	920 TWh/year	68254 TWh/year	370,41 TWh/year	882,8 TWh/year
Theoretical Technical Potential	304,13 TWh/year	----	----	----	----
Carnot Potential	----	279 TWh/year	13372 TWh/year	173,99 TWh/year	150,7 TWh/year
Dominant Industries in WHR	Steel and Iron; Non-metallic minerals (cement)	Steel and Iron; Non-metallic Minerals (cement); Food; Chemical	----	Steel and Iron; Non-metallic minerals (cement)	Steel and Iron; Non-metallic minerals (cement); Non-ferrous metals; Chemicals
Dominant Countries in WHR	Germany; France; Spain; Italy; United Kingdom	Germany; France; Spain; Italy; United Kingdom	----	Germany; France; Spain; Italy; United Kingdom	Germany; France; Spain; Italy; United Kingdom
Dominant temperature ranges in WHR	100 - 200°C; > 500°C	100 - 300°C; >300°C	100 - 299°C - Residential sector; > 300°C - Commercial, Industrial and Transport sector	100 - 300°C; >300°C	200 - 500°C; >500°C

ANNEX D

Table D.1. Main Processes used in several sectors of Industry - Adapted from [9], [10], [46]

Industry	Process	Heat Range [°C]	Heat classification [2]
Iron and Steel Production	Sinter process	1300 - 1480	HT
	Pelletisation plants – Induration process	Straight grate process: 1300 - 1350	HT
		Gate kiln process: 1250	HT
	Coke oven plants	1150 - 1350	ET
	Blast furnace – Hot Stoves	900 - 1500	ET
	Basic oxygen steelmaking	1200	ET
	Waste gas from coke oven	200	MT
	Blast furnace gas	450	ET
	Exhaust gases from Cowper regenerators	250	MT
	Exhaust gases from electric arc furnaces	204	MT
	Steam process - Boiler	340 - 450	MT/ET
Large Combustion Plants	Combustion/Gasification / Liquefaction process	430 - 630	ET
	Steam process - Boiler	Coal and Lignite fuels: 540 - 570	ET
		Liquid fuels: 120 - 140	MT

[2] Classification according to that adopted in [6]

	Co-generation/combined heat and power	100	BT
	Combined cycle plants	430 - 630	ET
Chemical and Petrochemical	Desulphurization	350 - 400	MT
	Conventional steam reforming - Primary and Secondary reforming	Primary: 400 - 600 Secondary: 400 - 600 Exhaust gas: 1000	ET ET ET
	Sulphuric Acid - Sulphur combustion SO_2 production	900 - 1500	ET
	Sulphuric Acid - Regeneration of spent acids SO_2 production	400 - 1000	ET
	Sulphuric Acid - Spent acid from TiO_2 production and roasting of metal sulphates	> 850	ET
	Sulphur burning process	145	MT
	Tank furnace process	430 - 650	ET
	Distillation	100 - 300	MT
	Stack of gas from crude distillation	156	MT
	Stack of gas from vacuum distillation	216	MT
	Exhaust from ethylene furnace	149	MT
Food	Seed oil extraction process	65	BT
	Solubilisation/alkalizing process	45 - 130	BT
	Utility processes -CHP	60 - 115	BT
	Heat recovery from cooling systems	50 - 60	BT

	Frying	180 - 200	MT
	Water vapor from evaporation and distillation	100	BT
Glass	Heating the furnaces and primary melting	750 - 1650	ET
Non-ferrous metals	Primary lead and secondary lead production	200 - 400	MT
	Smelting Process	400 - 1200	ET
	Zinc sulphide (sphalerite)	900 - 1000	ET
Cement	Kiln firing	> 2000	ET
	Clinker burning	1400 - 2000	ET
Pulp, Paper, and Board production	Kraft pulping process	155 - 175	MT
	Sulphate pulping process	800 - 1100	ET
	Mechanical pulping	95 - 125	BT/MT
	Papermaking and related processes	> 350	MT/ET
	Waste steam from slag flushing in furnace	95 - 100	BT
	Wastewater from slag flushing in furnace	65 - 85	BT
	Cooling water from furnace wall cooling	35 - 45	BT
Surface Treatment	Printing	700 - 800	ET
	Drying and curing	400 - 700	ET
	Manufacturing of Abrasives	In the drier: 35 - 110 For the exhaust air treatment: 700	BT ET
Textiles	Dirt removal	1200	ET
	Dyeing	80 - 100	BT

	Oxidation	750	ET
	Drying	130	MT
	Wastewater rejected from heat exchangers	58 - 66	BT
Waste Incineration	Drying and degassing	100 - 300	MT
	Pyrolysis	250 - 700	MT/ET
	Gasification	500 - 1600	ET
	Oxidation, Combustion	800 - 1450	ET
Waste Treatment	Thermal Treatment	Vitrification: 1300 - 1500 Sintering: 900 - 1200	ET ET
	Drying	100	BT
	Regeneration of carbon	650 - 1000	ET
	Incineration	850 - 1200	ET
	Catalytic combustion	200 - 600	MT/ET
Wood based panels production	Drying of wood fibres	60 - 220	BT/MT
	Pressing	100 - 260	MT
	Lamination	130 - 200	MT

ANNEX E

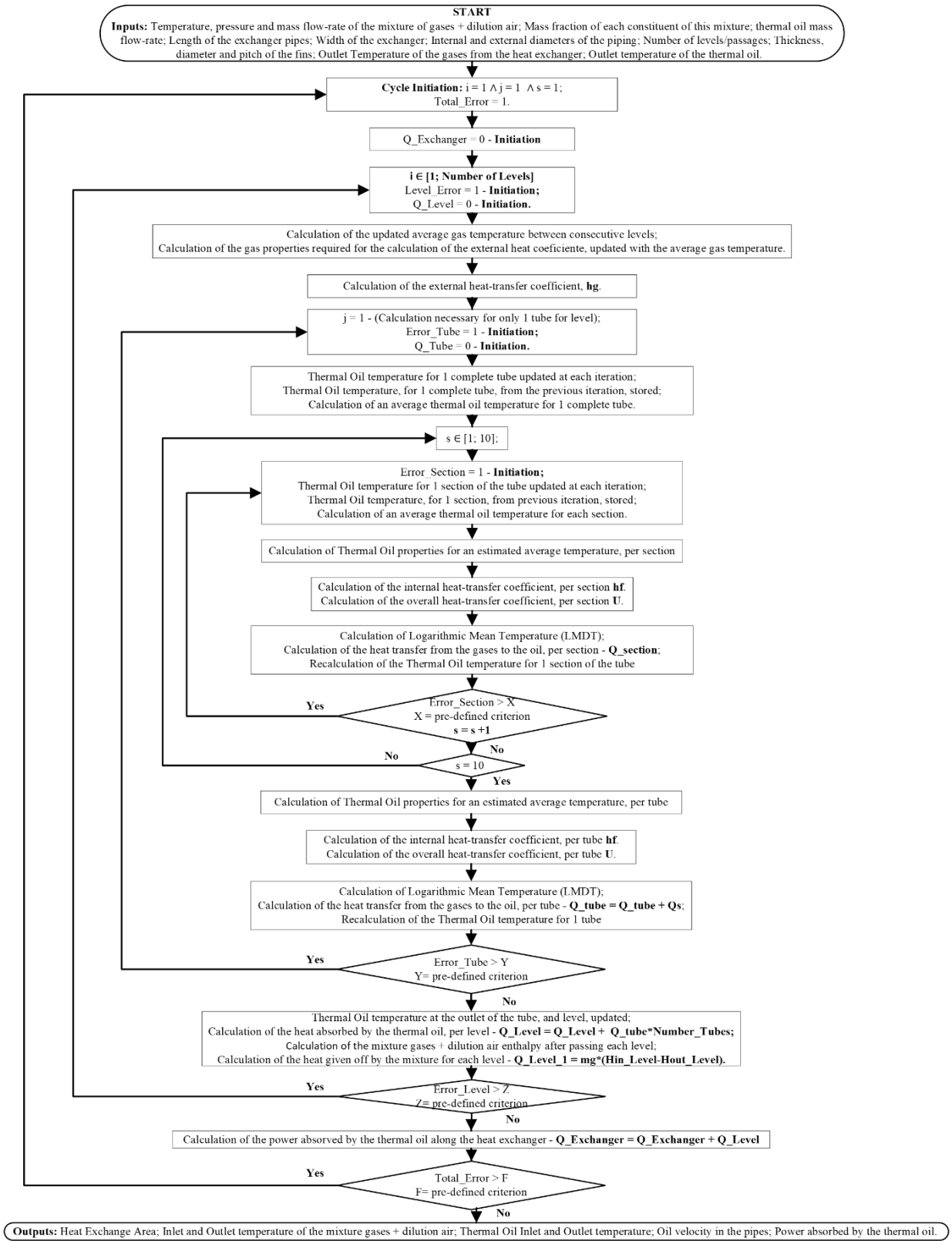
START
Inputs: Temperature, pressure and mass flow-rate of the mixture of gases + dilution air; Mass fraction of each constituent of this mixture; thermal oil mass flow-rate; Length of the exchanger pipes; Width of the exchanger; Internal and external diameters of the piping; Number of levels/passages; Thickness, diameter and pitch of the fins; Outlet Temperature of the gases from the heat exchanger; Outlet temperature of the thermal oil.
Cycle Initiation: i = 1 ∧ j = 1 ∧ s = 1;
Total_Error = 1.
Q_Exchanger = 0 - Initiation
i ∈ [1; Number of Levels]
Level_Error = 1 - Initiation;
Q_Level = 0 - Initiation.
Calculation of the updated average gas temperature between consecutive levels;
Calculation of the gas properties required for the calculation of the external heat coeficiente, updated with the average gas temperature.
Calculation of the external heat-transfer coefficient, hg.
j = 1 - (Calculation necessary for only 1 tube for level);
Error_Tube = 1 - Initiation;
Q_Tube = 0 - Initiation.
Thermal Oil temperature for 1 complete tube updated at each iteration;
Thermal Oil temperature, for 1 complete tube, from the previous iteration, stored;
Calculation of an average thermal oil temperature for 1 complete tube.
s ∈ [1; 10];
Error_Section = 1 - Initiation;
Thermal Oil temperature for 1 section of the tube updated at each iteration;
Thermal Oil temperature, for 1 section, from previous iteration, stored;
Calculation of an average thermal oil temperature for each section.
Calculation of Thermal Oil properties for an estimated average temperature, per section
Calculation of the internal heat-transfer coefficient, per section hf.
Calculation of the overall heat-transfer coefficient, per section U.
Calculation of Logarithmic Mean Temperature (LMDT);
Calculation of the heat transfer from the gases to the oil, per section - Q_section;
Recalculation of the Thermal Oil temperature for 1 section of the tube
Error_Section > X
X = pre-defined criterion
s = s +1
Yes
No
s = 10
No
Yes
Calculation of Thermal Oil properties for an estimated average temperature, per tube
Calculation of the internal heat-transfer coefficient, per tube hf.
Calculation of the overall heat-transfer coefficient, per tube U.
Calculation of Logarithmic Mean Temperature (LMDT);
Calculation of the heat transfer from the gases to the oil, per tube - Q_tube = Q_tube + Qs;
Recalculation of the Thermal Oil temperature for 1 tube
Error_Tube > Y
Y= pre-defined criterion
Yes
No
Thermal Oil temperature at the outlet of the tube, and level, updated;
Calculation of the heat absorbed by the thermal oil, per level - Q_Level = Q_Level + Q_tube*Number_Tubes;
Calculation of the mixture gases + dilution air enthalpy after passing each level;
Calculation of the heat given off by the mixture for each level - Q_Level_1 = mg*(Hin_Level-Hout_Level).
Error_Level > Z
Z= pre-defined criterion
Yes
No
Calculation of the power absorved by the thermal oil along the heat exchanger - Q_Exchanger = Q_Exchanger + Q_Level
Total_Error > F
F= pre-defined criterion
Yes
No
Outputs: Heat Exchange Area; Inlet and Outlet temperature of the mixture gases + dilution air; Thermal Oil Inlet and Outlet temperature; Oil velocity in the pipes; Power absorbed by the thermal oil.

ANNEX F

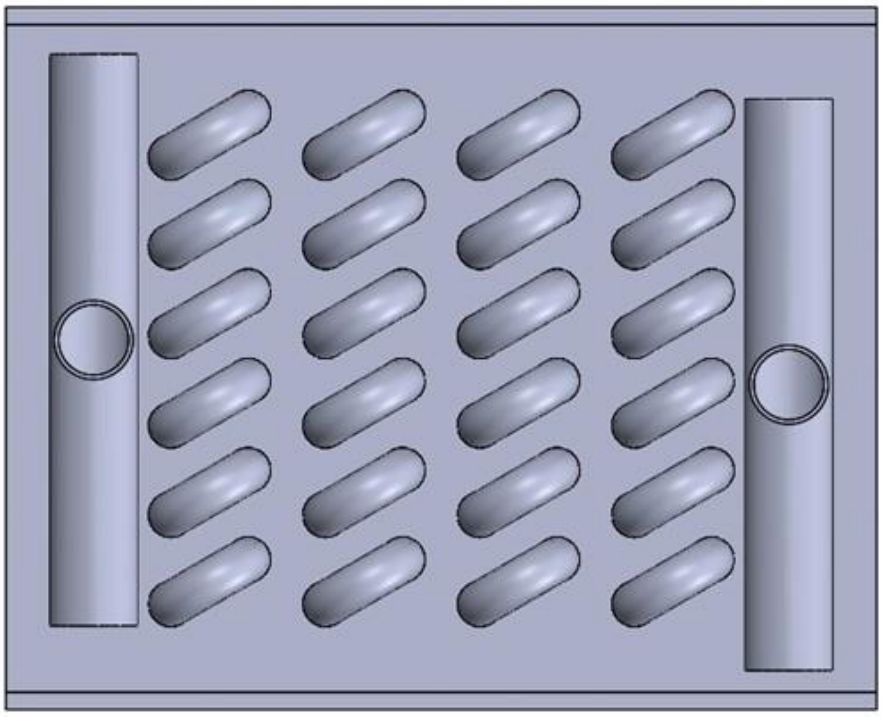

Figure F.1. Right side view of the heat exchanger.

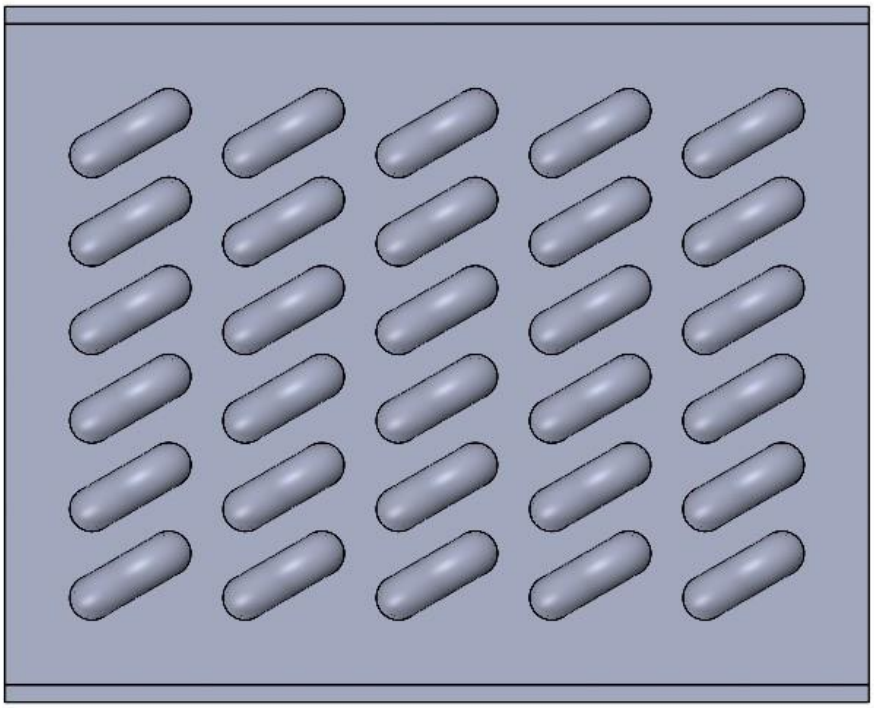

Figure F.2. Left side view of the heat exchanger.

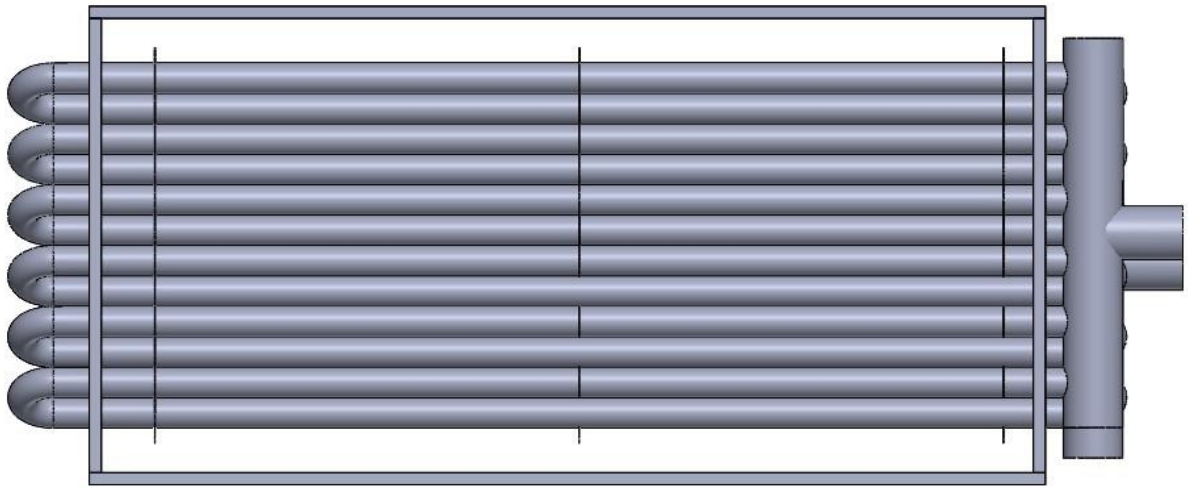

Figure F.3. Frontal view of the heat exchanger.

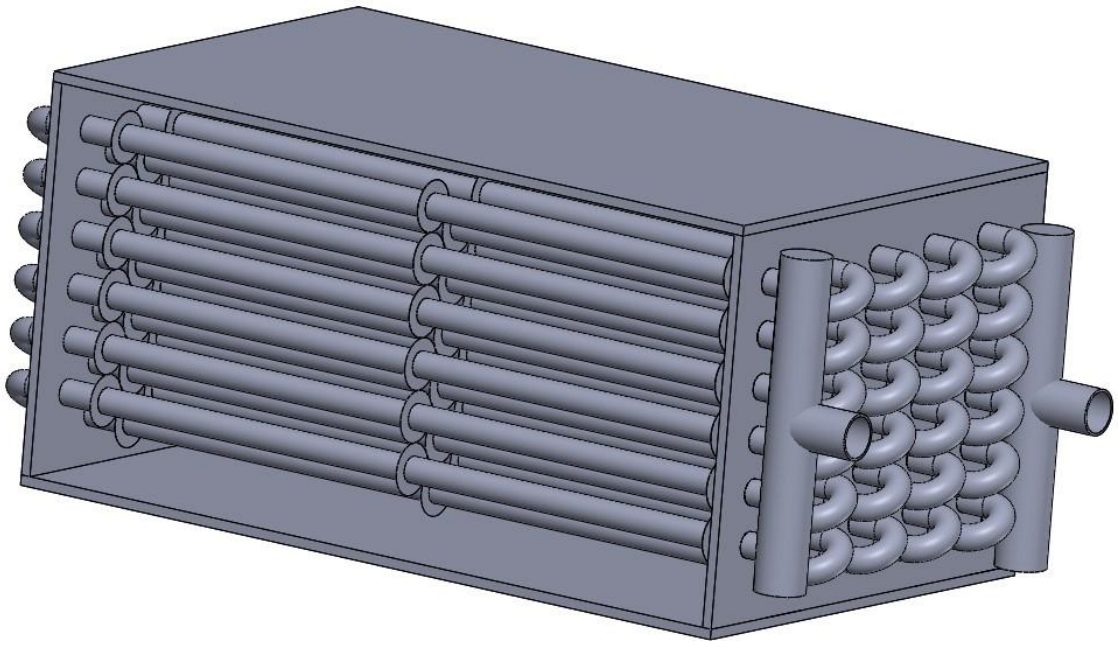

Figure F.4. Isometric view of the heat exchanger.

ANNEX G

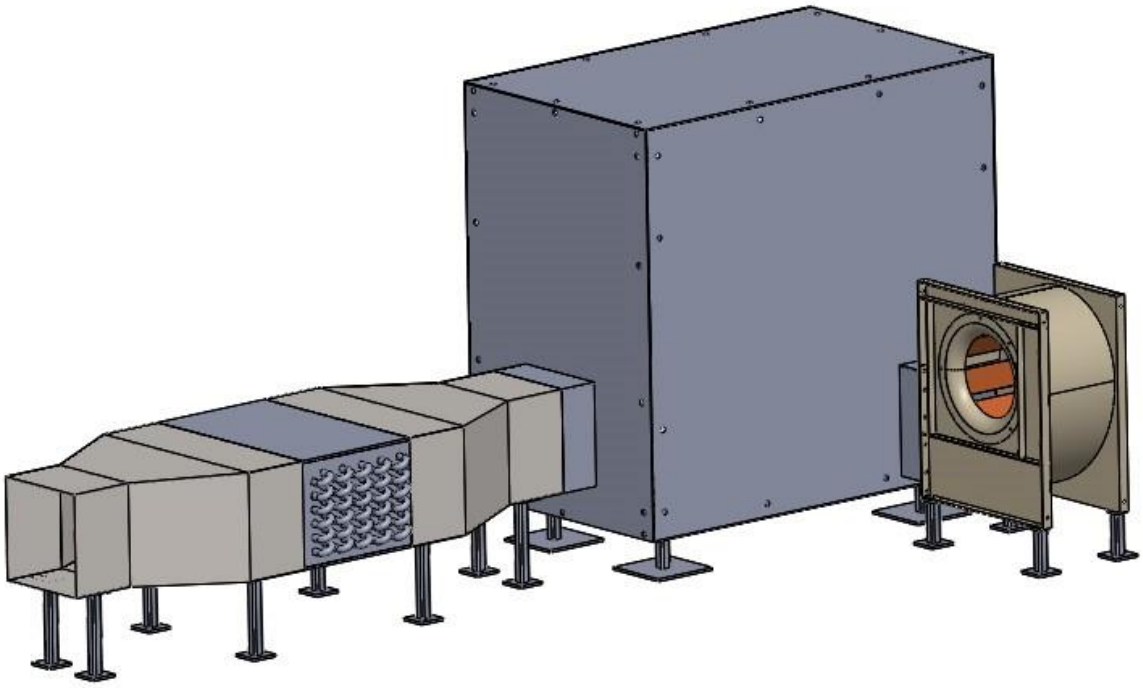

Figure G.1. Isometric view of the assembly.

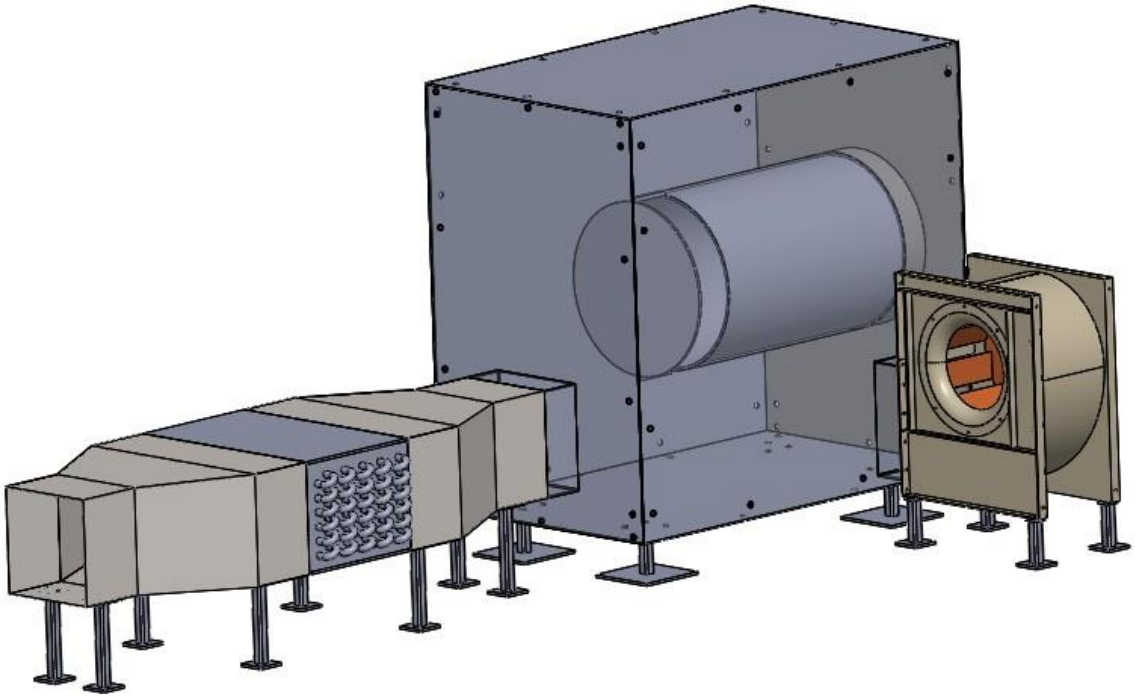

Figure G.2. Isometric view of the assembly - Internal detail of the **c**ombustion and mixing/dilution chamber .

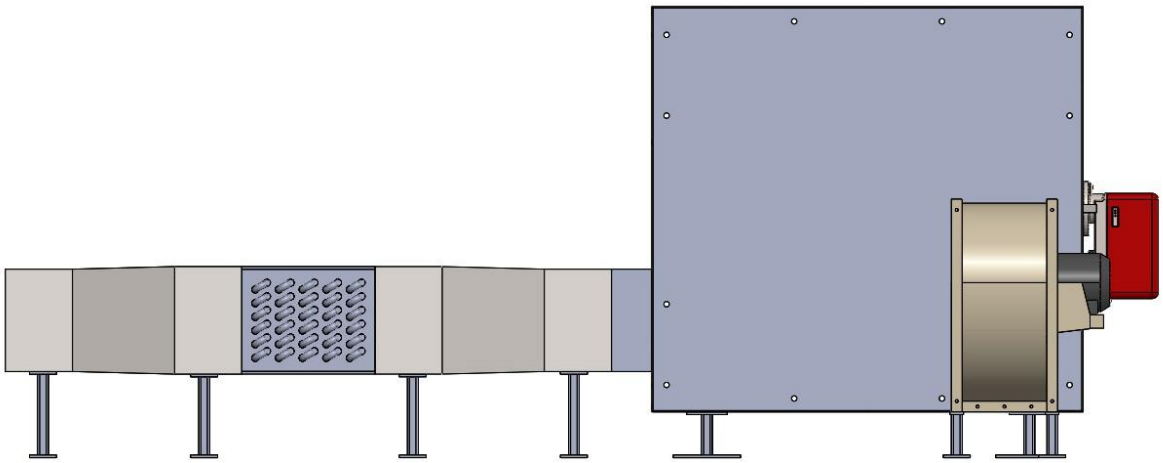

Figure G.3. Right view of the assembly.

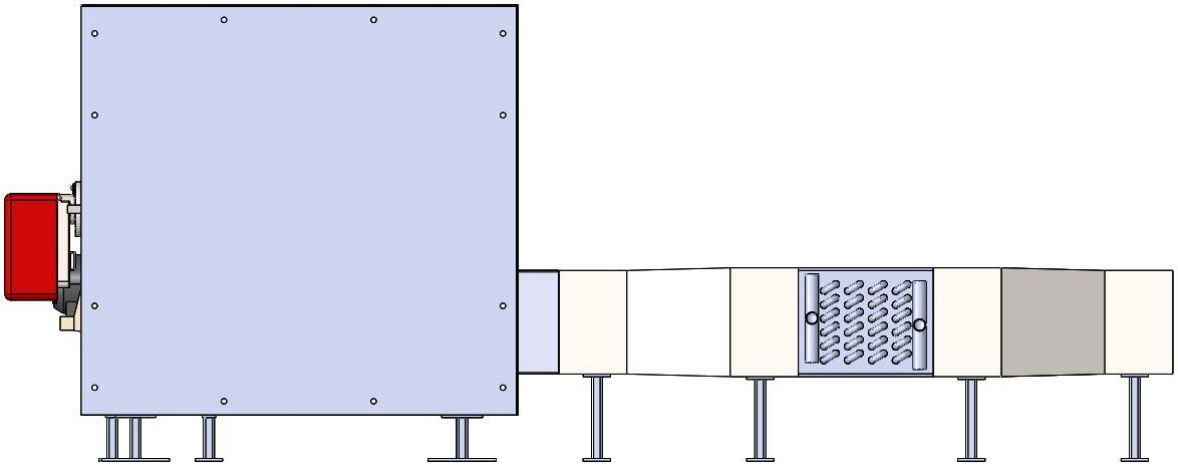

Figure G.4. Left view of the assembly.

APPENDIX A

The development of the algorithm for calculating the LHV of natural gas presents the following steps:

- **Step 1:** Input: Molar percentage of each constituent of the NG.
- **Step 2:** Calculation of the NG composition by weight:

It is necessary to start by knowing the theoretical stoichiometric equation for natural gas:

$$\begin{aligned}(n_{CH_4}CH_4 + n_{C_2H_6}C_2H_6 + n_{C_3H_8}C_3H_8 + n_{C_4H_{10i}}C_4H_{10i} + n_{C_4H_{10n}}C_4H_{10n} \\ + n_{C_5H_{12i}}C_5H_{12i} + n_{C_5H_{12n}}C_5H_{12n} + n_{C_6H_{14n}}C_6H_{14n} + n_{N_2}N_2 \\ + n_{CO_2}CO_2) + Z_{th}(O_2 + 3.76N_2) \rightarrow aCO_2 + bH_2O + cN_2\end{aligned} \quad (A.1)$$

By constructing a table with the molar percentage of each constituent as well as the number of atoms in each one, it is possible to obtain the weight composition of the natural gas.

Table A.1. Molar percentage of each constituent as well as the number of atoms in each one.

$N_{R.P}$	CH_4	C_2H_6	C_3H_8	$C_4H_{10}i$	C_4H_{10n}	C_5H_{12i}	C_5H1_{2n}	C_6H_{14n}	N_2	CO_2
	87.885%	**8.056%**	**1.378%**	**0.108%**	**0.158%**	**0.022%**	**0.018%**	**0.02%**	**1.088%**	**1.266%**
C	1	2	3	4	4	5	5	6	0	1
H	4	6	8	10	10	12	12	14	0	0
N	0	0	0	0	0	0	0	0	2	0
O	0	0	0	0	0	0	0	0	0	2

$$\begin{aligned}C &= 1 \times 0.87885 + 2 \times 0.08056 + 3 \times 0.01378 + 4 \times 0.00108 \\ &\quad + 4 \times 0.00158 + 5 \times 0.00022 + 5 \times 0.00018 + 6 \times 0.0002 \\ &\quad + 1 \times 0.01266 \\ H &= 4 \times 0.87885 + 6 \times 0.08056 + 8 \times 0.01378 + 10 \times 0.00108 \\ &\quad + 10 \times 0.00158 + 12 \times 0.00022 + 12 \times 0.00018 \\ &\quad + 14 \times 0.0002 \\ N &= 2 \times 0.00018 \\ O &= 2 \times 0.01266\end{aligned} \quad (A.2)$$

Thus, obtaining a weighted composition of the natural gas:

$$C_{1.10781}H_{4.1432}N_{0.02176}O_{0.02532} \tag{A.3}$$

- **Step 3:** Obtain the stoichiometric coefficients of combustion:

$$C_{1.10781}H_{4.1432}N_{0.02176}O_{0.02532} + Z_{th}(O_2 + 3.76N_2) \rightarrow aCO_2 + bH_2O + cN_2 \tag{A.4}$$

Table A.2. Number of moles of each constituent.

	a*CO_2	b*H_2O	c*N_2	Z_{th}
C	1	0	0	0
H	0	2	0	0
N	0	0	2	-8
O	2	1	0	-2

Table A.3. Molar composition of natural gas.

Natural Gas
C = 1.10781
H = 4.1432
N = 0.02176
O = 0.02532

$$A = \begin{bmatrix} 1 & 0 & 0 & 0 \\ 0 & 2 & 0 & 0 \\ 0 & 0 & 2 & -8 \\ 2 & 1 & 0 & -2 \end{bmatrix} \tag{A.5}$$

$$B = \begin{bmatrix} 1.10781 \\ 4.1432 \\ 0.02176 \\ 0.02532 \end{bmatrix} \tag{A.6}$$

$$C = A^{-1} \cdot B \Leftrightarrow \begin{Bmatrix} a \\ b \\ c \\ Z_{th} \end{Bmatrix} = \begin{bmatrix} 1.10781 \\ 2.0716 \\ 8.023252 \\ 2.13095 \end{bmatrix} \tag{A.7}$$

- **Step 4:** Number of moles of reactants and products:

Moles of Reactants:

$$\begin{cases} n_{CH_4} = 0.87885 \\ n_{C_2H_6} = 0.08056 \\ n_{C_3H_8} = 0.01378 \\ n_{C_4H_{10i}} = 0.00108 \\ n_{C_4H_{10n}} = 0.00158 \\ n_{C_5H_{12i}} = 0.00022 \\ n_{C_5H_{12n}} = 0.00018 \\ n_{C_6H_{14n}} = 0.0002 \\ n_{N_2} = 0.00018 + Z_{th} \times 3.76 \\ n_{CO_2} = 0.01266 \\ n_{O_2} = Z_{th} \times 1 \end{cases} \quad [kmol] \tag{A.8}$$

Moles of Products:

$$\begin{cases} n_{CO_2} = a = 1.10781 \\ n_{H_2O} = b = 2.0716 \\ n_{N_2} = c = 8.023252 \end{cases} \quad [mol] \tag{A.9}$$

- **Step 5:** Enthalpy of formation of reactants at 298.15K:

$$\begin{cases} \Delta_f H°_{CH_4} = -74.87 \\ \Delta_f H°_{C_2H_6} = -84.68 \\ \Delta_f H°_{C_3H_8} = -103.85 \\ \Delta_f H°_{C_4H_{10i}} = -134.62 \\ \Delta_f H°_{C_4H_{10n}} = -125.79 \\ \Delta_f H°_{C_5H_{12i}} = -153.17 \\ \Delta_f H°_{C_5H_{12n}} = -146.25 \\ \Delta_f H°_{C_6H_{14n}} = -166.89 \\ \Delta_f H°_{N_2} = 0 \\ \Delta_f H°_{CO_2} = -393.51 \\ \Delta_f H°_{O_2} = 0 \\ \Delta_f H°_{H_2O} = -241.83 \end{cases} \quad [\frac{kJ}{kmol}] \tag{A.10}$$

- **Step 6:** Molar Mass of Reactants:

$$\begin{cases} M_{CH_4} = 0.016043 \\ M_{C_2H_6} = 0.030070 \\ M_{C_3H_8} = 0.044097 \\ M_{C_4H_{10i}} = 0.058124 \\ M_{C_4H_{10n}} = 0.058124 \\ M_{C_5H_{12i}} = 0.072151 \\ M_{C_5H_{12n}} = 0.072151 \\ M_{C_6H_{14n}} = 0.086 \\ M_{N_2} = 0.00018 + Z_{th} \times 3.76 \\ M_{CO_2} = 0.01266 \end{cases} \quad [kg/mol] \tag{A.11}$$

- **Step 7:** Calculate the Molar Mass of NG:

$$M_{GN} = \sum_{Natural\ Gas} n_i \times M_i = 0.0182 \left[\frac{kg}{mol}\right] \tag{A.12}$$

- **Step 8:** Calculation of the Lower Calorific Value:

$$LHV = \frac{\left(\sum_{Reactants} n_i \times \Delta_f H°_i - \sum_{Products} n_j \times \Delta_f H°_j\right)}{M_{GN}} = 47.13177 \left[\frac{MJ}{kg}\right] = 857426.67005 \left[\frac{kJ}{kmol}\right] = 857.427 \left[\frac{MJ}{kmol}\right] \tag{A.13}$$

APPENDIX B

To develop the algorithm which allows the calculation of the air flow to be blown and/or the temperature at the outlet for a given flow rate, the following steps are followed:

- **Step 1:** Input: Lower Calorific Value. Molar percentage of each constituent of NG.

Calculation of the molar flow rate of natural gas:

$$\dot{n}_{NG}[kmol/s] = \frac{P_{Burner}}{LHV}\left[\frac{kW}{kJ/kmol}\right] \tag{B.1}$$

Calculation of the number of moles of each constituent of natural gas, using the molar flow rate of natural gas and the molar percentage of each constituent.

- **Step 2:** Calculation of the NG composition by weight:

In a similar way to Step 2 of the LHV calculation, we begin by constructing a table to obtain the weight composition of the natural gas, this time considering the molar flow rate of natural gas, which varies according to the power of the burner and the lower calorific value of the natural gas.

Table B.1. Molar percentage of each constituent as well as the number of atoms in each one.

$\dot{n}_{GN} \times$	CH_4	C_2H_6	C_3H_8	$C_4H_{10i}i$	C_4H_{10n}	C_5H_{12i}	C_5H_{12n}	C_6H_{14n}	N_2	CO_2
$N_{R.P}$	**87.885%**	**8.056%**	**1.378%**	**0.108%**	**0.158%**	**0.022%**	**0.018%**	**0.02%**	**1.088%**	**1.266%**
C	1	2	3	4	4	5	5	6	0	1
H	4	6	8	10	10	12	12	14	0	0
N	0	0	0	0	0	0	0	0	2	0
O	0	0	0	0	0	0	0	0	0	2

- **Step 3:** Obtain the stoichiometric coefficients for the theoretical combustion of natural gas. Performing the stoichiometric equation on a unit basis of 1s:

$$\begin{aligned} n_{GN} \times (&n_{CH_4}CH_4 + n_{C_2H_6}C_2H_6 + n_{C_3H_8}C_3H_8 + n_{C_4H_{10i}}C_4H_{10i} \\ &+ n_{C_4H_{10n}}C_4H_{10n} + n_{C_5H_{12i}}C_5H_{12i} + n_{C_5H_{12n}}C_5H_{12n} \\ &+ n_{C_6H_{14n}}C_6H_{14n} + n_{N_2}N_2 + n_{CO_2}CO_2) + Z_{th}(O_2 + 3.76N_2) \\ &\rightarrow aCO_2 + bH_2O + cN_2 \end{aligned} \tag{B.2}$$

- **Step 4:** Obtain the stoichiometric coefficients for the actual combustion of natural gas, with an imposed excess air.

$$\begin{aligned} n_{GN} \times (& n_{CH_4} CH_4 + n_{C_2H_6} C_2H_6 + n_{C_3H_8} C_3H_8 + n_{C_4H_{10i}} C_4H_{10i} \\ & + n_{C_4H_{10n}} C_4H_{10n} + n_{C_5H_{12i}} C_5H_{12i} + n_{C_5H_{12n}} C_5H_{12n} \\ & + n_{C_6H_{14n}} C_6H_{14n} + n_{N_2} N_2 + n_{CO_2} CO_2) \\ & + \lambda \times Z_{th}(O_2 + 3.76N_2) \rightarrow aCO_2 + bH_2O + cN_2 + dO_2 \end{aligned} \quad \text{(B.3)}$$

- **Step 5:** Number of moles of reactants and products.
  Same step as in APPENDIX A.
- **Step 6:** Calculate the mole fraction of the products:

$$\begin{cases} x_{CO_2} = \dfrac{n_{CO_2}}{n_{CO_2} + n_{H_2O} + n_{N_2} + n_{O_2}} \\ x_{H_2O} = \dfrac{n_{H_2O}}{n_{CO_2} + n_{H_2O} + n_{N_2} + n_{O_2}} \\ x_{N_2} = \dfrac{n_{N_2}}{n_{CO_2} + n_{H_2O} + n_{N_2} + n_{O_2}} \\ x_{O_2} = \dfrac{n_{O_2}}{n_{CO_2} + n_{H_2O} + n_{N_2} + n_{O_2}} \end{cases} \quad \text{(B.4)}$$

- **Step 7:** Enthalpy of formation of reactants at 298.15 K:

$$\begin{cases} \Delta_f H°_{CH_4} = -74.87 \\ \Delta_f H°_{C_2H_6} = -84.68 \\ \Delta_f H°_{C_3H_8} = -103.85 \\ \Delta_f H°_{C_4H_{10i}} = -134.62 \\ \Delta_f H°_{C_4H_{10n}} = -125.79 \\ \Delta_f H°_{C_5H_{12i}} = -153.17 \\ \Delta_f H°_{C_5H_{12n}} = -146.25 \\ \Delta_f H°_{C_6H_{14n}} = -166.89 \\ \Delta_f H°_{N_2} = 0 \\ \Delta_f H°_{CO_2} = -393.51 \\ \Delta_f H°_{O_2} = 0 \\ \Delta_f H°_{H_2O} = -241.83 \end{cases} \left[\frac{kJ}{kmol}\right] \quad \text{(B.5)}$$

- **Step 8:** Calculation of the partial pressure of the products:

$$\begin{cases} pp_{CO_2} = n_{CO_2} \times 101325 \\ pp_{H_2O} = n_{H_2O} \times 101325 \\ pp_{N_2} = n_{N_2} \times 101325 \\ pp_{O_2} = n_{O_2} \times 101325 \end{cases} \quad \text{(B.6)}$$

- **Step 9:** Calculation of Adiabatic Flame Temperature:

By imposing in the algorithm, a stopping criterion $H_P^\circ - H_R^\circ < 10^{-7}$ and already knowing the enthalpy of formation of the reactants at 298.15 K, it is possible with recourse to an iterative cycle to obtain the value of the temperature for which the enthalpy of formation of the products allows to fulfil the imposed criterion.

To obtain the enthalpy properties of each product we use the MATLAB add-on: "CoolProp". For the add-on to return the values necessary for the calculation it is essential to provide the value of the temperature (which is the calculation objective) and the partial pressure of each product that has already been calculated.

Knowing that the reactants enter at a temperature equal to 298.15 K:

$$\begin{aligned} H_R^\circ = n_{GN} \times (& n_{CH_4} \times \Delta_f H^\circ{}_{CH_4} + n_{C_2H_6} \times \Delta_f H^\circ{}_{C_2H_6} + n_{C_3H_8} \times \Delta_f H^\circ{}_{C_3H_8} \\ & + n_{C_4H_{10i}} \times \Delta_f H^\circ{}_{C_4H_{10i}} + n_{C_4H_{10n}} \times \Delta_f H^\circ{}_{C_4H_{10n}} \\ & + n_{C_5H_{12i}} \times \Delta_f H^\circ{}_{C_5H_{12i}} + n_{C_5H_{12n}} \times \Delta_f H^\circ{}_{C_5H_{12n}} \\ & + n_{C_6H_{14n}} \times \Delta_f H^\circ{}_{C_6H_{14n}} + n_{N_2} \times \Delta_f H^\circ{}_{N_2} + n_{CO_2} \times \Delta_f H^\circ{}_{CO_2}) \\ & + Z_{th} \times 3.76 N_2 \times \Delta_f H^\circ{}_{N_2} + Z_{th} \times \Delta_f H^\circ{}_{O_2} \end{aligned} \quad \text{(B.7)}$$

$$\begin{aligned} H_P^\circ = n_{CO_2} \times & \left[\Delta_f H^\circ{}_{CO_2} + \left(\tilde{h}^\circ_{CO_2@Tflame} - \tilde{h}^\circ_{CO_2@298.15\,K}\right)\right] \\ & + n_{H_2O} \times \left[\Delta_f H^\circ{}_{H_2O} + \left(\tilde{h}^\circ_{H_2O@Tflame} - \tilde{h}^\circ_{H_2O@298.15\,K}\right)\right] \\ & + n_{O_2} \times \left[\Delta_f H^\circ{}_{O_2} + \left(\tilde{h}^\circ_{O_2@Tflame} - \tilde{h}^\circ_{O_2@298.15\,K}\right)\right] \\ & + n_{N_2} \times \left[\Delta_f H^\circ{}_{N_2} + \left(\tilde{h}^\circ_{N_2@Tflame} - \tilde{h}^\circ_{N_2@298.15\,K}\right)\right] \end{aligned} \quad \text{(B.8)}$$

When the criterion is met, the value of the adiabatic flame temperature is obtained.

- **Step 10:** Energy balance between combustion products at adiabatic flame temperature and dilution air at 25°C, assuming that the combustion chamber is adiabatic:

$$\begin{aligned} n_{AR,Dilution} \times \left(H_{AR,Diluição@Toutlet} - H_{AR,Diluição@298,15}\right) \\ = a \times \left(H_{CO_2@Tflame} - H_{CO_2@Toutlet}\right) \\ + b \times \left(H_{H_2O@Tflame} - H_{H_2O@Toutlet}\right) \\ + c \times \left(H_{N_2@Tflame} - H_{N_2@Toutlet}\right) \\ + d \times \left(H_{O_2@Tflame} - H_{O_2@Toutlet}\right) \end{aligned} \quad \text{(B.9)}$$

- **Step 11.1:** If the airflow to be ventilated is required to obtain a certain outlet temperature:

$$\begin{aligned} n_{Air,Dilution} \times \left(H_{Air,Dilution@Toutlet} - H_{Air,Dilution@298,15}\right) \\ = a \times \left(H_{CO_2@Tflame} - H_{CO_2@Toutlet}\right) \\ + b \times \left(H_{H_2O@Tflame} - H_{H_2O@Toutlet}\right) \\ + c \times \left(H_{N_2@Tflame} - H_{N_2@Toutlet}\right) \\ + d \times \left(H_{O_2@Tflame} - H_{O_2@Toutlet}\right) \end{aligned} \quad \text{(B.10)}$$

$$\Leftrightarrow n_{Air,Dilution} = \frac{\begin{aligned}(a \times \left(H_{CO_2@Tflame} - H_{CO_2@Toutlet}\right) + b \times \left(H_{H_2O@Tflame} - H_{H_2O@Toutlet}\right) + \\ c \times \left(H_{N_2@Tflame} - H_{N_2@Toutlet}\right) + d \times \left(H_{O_2@Tflame} - H_{O_2@Toutlet}\right))\end{aligned}}{\left(H_{Air,Dilution@Toutlet} - H_{Air,Dilution@298,15}\right)} \quad \text{(B.11)}$$

$$m_{Air,Dilution} = n_{Air,Dilution} \times M_{Air} \quad \text{(B.12)}$$

$$V_{Air,Dilution} = m_{Air,Dilution}/\rho_{Air} \quad \text{(B.13)}$$

- **Step 11.2:** If the outlet temperature is required for a particular flow rate:

It is necessary to implement an iterative cycle that allows to obtain the outlet temperature. Thus, as in the calculation of the adiabatic flame temperature, it is necessary to impose a stopping criterion. Here, two energy balances are performed, one at the inlet and one at the outlet. If the difference between the two is less than 10^{-7}, the temperature obtained in the cycle is the temperature of the mixture at the outlet.